ELSEVIER

Contents lists available at ScienceDirect

Coordination Chemistry Reviews

journal homepage: www.elsevier.com/locate/ccr



Planar, curved and twisted molecular nanographenes: Reduction-induced alkali metal coordination [☆]



Zheng Zhou a,b, Marina A. Petrukhina b,*

ARTICLE INFO

Article history: Received 1 March 2023 Received in revised form 22 March 2023 Accepted 23 March 2023

Keywords: Alkali metal coordination Carbon π-bowls Molecular nanocarbons Nanographenes Non-planar π-ligands

ABSTRACT

Planar and curved polycyclic aromatic hydrocarbons (PAHs) attract significant attention as molecular models of fullerenes, carbon nanotubes, and graphene, thus stimulating broad investigation of chemical reactivity and materials applications of designed nanocarbon π -systems. Non-planar molecular nanographenes (**NGs**) recently emerge as advanced anode materials in energy storage, showing high reduction limits and enhanced alkali metal intercalation levels. However, the lack of direct structure–property correlations in such complex hybrid systems impedes their further development and utilization. With a focus on alkali-metal-induced reduction of selected PAHs, we herein review original metal binding and intercalation trends, site specific coordination, and distinct carbon framework responses to stepwise electron uptake. Small planar graphene fragments, like triphenylene and coronene, are compared to π -expanded hexabenzocoronenes, followed by the discussion of bowl-shaped corannulene, sumanene and other carbon bowls, as well as bent, warped, and twisted molecular nanographenes. The effect of size, symmetry, and framework topology along with the structural deformation of carbon backbones upon reduction are analyzed, using recent crystallographic examples of alkali-metal intercalated products. The revealed insights into the structures, binding, and metal intercalation in molecular nanographenes should stimulate their future applications as new functional materials.

© 2023 Elsevier B.V. All rights reserved.

Contents

	Introduction	
2.	Planar PAHs as graphene fragments	2
3.	Adding curvature: Bowl-shaped π -ligands	
4.	Bent and twisted molecular nanographenes	10
5.	Conclusions.	13
	Credit authorship contribution statement	14
	Declaration of Competing Interest	14
	Acknowledgements	14
	References	14

1. Introduction

The discovery and wide-ranging applications of curved carbon allotropes, fullerenes [1] and carbon nanotubes [2], sparked the development of synthetic methods for the controlled preparation of their non-planar molecular fragments with defined structures

E-mail address: mpetrukhina@albany.edu (M.A. Petrukhina).

and compositions. A large number of carbon bowls or π -bowls (also referred to as fullerene fragments or buckybowls) with different symmetry, size and depth became available due to the efforts of multiple synthetic groups [3–6]. In addition, a great variety of carbon hoops and belts with different dimensions and frameworks, considered as fragments of carbon nanotubes, were creatively designed [7–11]. Exploration of these classes of non-planar polycyclic aromatic hydrocarbons (PAHs) was booming in recent years with a focus on their unusual structures, aromaticity, optical, conductive, and supramolecular properties [12–15].

^a Interdisciplinary Materials Research Center, School of Materials Science and Engineering, Tongji University, Shanghai 201804, China

^b Department of Chemistry, University at Albany, State University of New York, 1400 Washington Avenue, Albany, NY 12222, USA

 $[\]mbox{\ensuremath{^{\, \pm}}}$ This paper is part of the special issue The Female Stars of Coordination Chemistry.

^{*} Corresponding author.

While the presence of five-membered rings embedded into sp²-carbon lattice introduces a positive Gaussian curvature [16–21], incorporation of seven- or eight-membered rings provides access to new warped and contorted π -systems with negative Gaussian curvatures [22–28]. The fast development of modern synthetic methods coupled with incredible imaginative creativity of synthetic chemists enabled the preparation of new three-dimensional carbon architectures with unique non-planar topologies, such as interlocked catenanes, knots, cages [29–34], as well as nanotube segments [35–37], helicenes [38–43], and polymeric carbon frameworks [44–46]. The chemistry of curved and twisted molecular nanocarbons continues to evolve very rapidly driven not only by their structural originality and fundamental interest but also by emerging practical applications such as optoelectronic, semiconductor, superconductor, and sensing applications [47–51].

Importantly, the contorted π -surfaces and internal porosity of curved nanocarbon hosts are known to facilitate efficient metal ion transport [52]. Moreover, bent and twisted PAHs often exhibit higher reduction limits and increased metal intercalation [53,54] coupled with improved stability and higher capacity compared to conventional graphite anodes [55-60]. For example, the anode material fabricated from corannulene, one of the smallest subunits of the C₆₀-fullerene that retains curvature, showed a high reversible lithium capacity (602 mAh/g), which is almost twice as high as the theoretical capacity of the commonly used fully lithiated planar graphite material (LiC₆, 372 mAh/g) [55]. In addition, contorted hexabenzocoronene (c-HBC) with a wire-shaped solid-state packing provided excellent conductivity and porous channels for Li+ ion transport during the charging/discharging process, revealing a single-step Li⁺ ion insertion behavior with a specific capacity of 267 mA·h/g and recovery capacity of 236 mA·h/g at 30 cycles (at 400 mA/g) [58]. The use of different carbon hosts for lithium-ion intercalation with potential application in lithium-ion batteries (LIB) is rapidly expanding to include new PAHs with a diverse range of framework topologies. For instance, large [6]cyclo2,7napththylene macrocycle ([6]CNAP, C₆₀H₄₀) exhibits the high capacity recorded at 727 mA·h/g with a reversible capacity of 593 mA·h/g after 65 cycles (at 425 mA/g) [56]. A trimeric hexabenzocoronene derivative with a 3D fan-like geometry shows a significantly enhanced LIB anode charge capacity of 950 mA·h/g with stability over 250 charge-discharge cycles [57]. These recent examples prompt special interest in the wide investigation of metal ion intercalation within different nanocarbon hosts combining the embedded non-planarity and π -surface extension with controlled molecular compositions (generally referred to as molecular nanographenes, NGs). However, while the number of nanographene materials probed in energy storage devices is constantly increasing, the fundamental studies on their reduction-induced metal coordination and reversible intercalation remain limited. More insights into structures and properties of alkali metaldoped hybrid products are needed in order to reveal their structure-property correlations and boost their material performance.

In this review, we analyze the trends in alkali metal coordination of a variety of molecular nanographenes with different compositions, dimensions, and carbon frameworks, focusing on the crystallographically confirmed examples of alkali metal intercalated products. Specifically, the effect of the framework topology, charge and ion size on trends in alkali metal binding and structural responses of π -hosts are discussed.

2. Planar PAHs as graphene fragments

The reduction of planar PAHs, serving as molecularly defined fragments of a 2D graphene, attracts significant attention from both fundamental and applied viewpoints. The resulting materials

exhibit intriguing electronic [61,62], conducting [63], and magnetic properties [64–68]; however, in-depth structure-property relationships are often impaired due to challenges with preparation of pure crystalline solids. During the last three decades, chemical reduction of planar PAHs with alkali metals coupled with the X-ray structural characterization of their products was reported for naphthalene [69,70], anthracene [71,72], phenalenyl [73], pyrene [74–77], perylene [78], tetracene [79], etc. Moreover, fusion of ring defects (four/five-membered rings) or introduction of peripheral phenyl rings enriched the diversity of PAHs and broadened this chemistry to include biphenylene [80], rubrene [81], fluoranthene [82], indenofluorene [83], decacyclene [79], and phenylene-tetracene [84–86]. In most reported π -complexes, the metal ions are bound to the edge of the mono-reduced PAH core to afford discrete or 1D columnar structures [74,87]. In contrast, the products of the doubly-reduced PAHs can also form sandwiched or 1D herringbone solid-state structures [72,73,83]. Upon one or two electron uptake, the PAH core remains almost planar, while the existence of ring defects or additional peripheral rings could lead to a more pronounced core curvature [79,81]. We contributed to these studies by adding X-ray structural characterization of several products stemming from alkali metal-induced reduction of planar PAHs with increasing surface size, as discussed below.

The reduction chemistry of **triphenylene** ($C_{18}H_{12}$, **TP**) was the subject of extensive investigations over several decades [88–98]. Due to its D_{3h} symmetry, the HOMO and LUMO of triphenylene are doubly degenerate, enabling a potential triplet ground state upon a two-fold reduction [96]. This triggered extensive EPR spectroscopy investigations [89,90,95]; however, the earlier studies remained focused on *in situ* generated mono-reduced **TP** and were unable to provide any specifics on coordination environment of the resulting radicals. The first crystal structure of the triphenylide-based molecular solid was reported only in 2017 [99]. The mono-reduced triphenylene isolated as $[\{K_2^*(DME)\}(TP^-)_2]$ showed the Mott insulator properties with strong antiferromagnetic coupling. This structure–property correlation study inspired the exploration of chemical reduction behavior of **TP** using different alkali metals, ranging from sodium to cesium.

In the course of our chemical reduction study [100], a series of the triphenylide-based products was prepared as single-phase crystalline solids such as [{Na*(18-crown-6)(THF)₂}(TP^-)] and [{M*(18-crown-6))(TP^-)] with M = K, Rb, and Cs. Their successful X-ray structural characterization revealed distinct variations in alkali metal ion coordination of the TP radical-anion. While the smaller Na* ion avoids direct coordination (Fig. 1a), the larger K*, Rb*, and Cs* ions favor the formation of π -complexes causing a notable geometry distortion of a rather rigid TP framework.

In $[\{K_2^+(DME)\}(TP^{--})_2]$ [99], the two independent K^+ ions are bound to two peripheral six-membered rings in η^3 - and η^6 fashions (Fig. 1b), with one additional contact of the K1 ion to the adjacent TP- anion. In all complexes reported in our group, one of the peripheral six-membered rings of TP- is engaged in metal binding which varies from a η^3 -mode for K⁺ ion (3.151(4)–3.262(4) Å) to a more symmetric η^6 -coordination for larger Rb⁺ (3.191(3)–3.645(3) Å) and Cs^+ (3.257(1)-3.761(2) Å) ions. Moving down the group, the metal-to-centroid distance becomes longer (3.075(4) to 3.215(2) Å) in accordance with the ion size increase. Furthermore, a good fit of the K⁺ ion within the cavity of the secondary 18-crown-6 ligand enables additional K...C contacts (3.407(4) Å) to the neighboring triphenylide anion, thus resulting in the 1D chain propagation. In contrast, the inability of larger Rb⁺ and Cs⁺ ions to fit inside the 18-crown-6 cavity results in their full entrapment between the two ligand decks, thus disabling additional cation... π contacts in both solids. Nevertheless, the propagation of 1D columns in the heavy alkali metal complexes occurs through $C-H\cdots\pi$ interactions

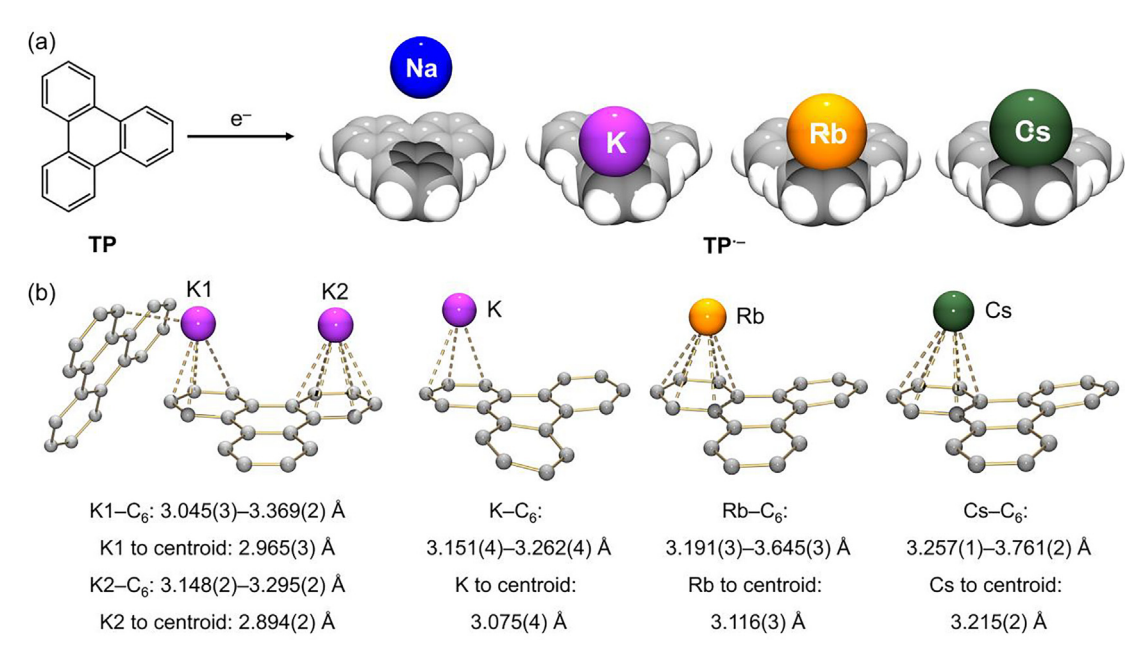


Fig. 1. (a) Chemical reduction of TP to afford the radical-anions, (b) coordination of TP⁻ with K*, Rb*, and Cs* ions.

between the triphenylide anions and $\{M^{+}(18\text{-crown-6})\}\ (M=Rb\ and\ Cs)$ cations. Interestingly, DFT calculations show that the charge transfer is ion size-dependent and drops from loss of $\sim 17\%$ for K⁺ to only $\sim 1\%$ for Cs⁺.

As illustrated for the series $[\{M^{+}(18-crown-6)\}(TP^{-})]$ (M = K, Rb, and Cs), the variation in primary alkali metal coordination is responsible for notable differences in the secondary microenvironment and solid-state packing of otherwise similar building units. In turn, the observed solid-state structure variations account for a distinct difference in magnetic properties of complexes with the same composition. The rubidium(I) and cesium(I) products show magnetic behavior typical of a Heisenberg spin-1/2 chain, wherein a broad maximum is followed by AFM ordering at 3.8 K and 2.2 K, respectively. The lack of such ordering for the potassium(I) product is rationalized by different structural organization of the TP radical-anions in the π -complexes with K^+ , Rb^+ and Cs^+ counterions. Thus, modulation of the metal ion size can serve as a tool for tuning magnetic interactions between the radicals in the solid-state, but structure-property correlations are needed for interpreting magnetic behavior.

Coronene ($C_{24}H_{12}$, **CON**) is often considered as a primary model of a graphene sheet and thus attracts significant attention from a broad chemical community [101–108]. Coronene with a D_{6h} symmetry is capable of acquiring up to two electrons upon reduction [109]. In contrast to the mono-reduced **CON** (*vide infra*), no crystallographically confirmed examples of its doubly-reduced products are yet reported.

The mono-reduced **CON** is known to exist in its "naked" form with sodium counterions [110], while heavier alkali metals tend to form π -complexes with **CON**⁻⁻ (Fig. 2a). In the first structurally characterized complex reported in 1994, [{K*(TMEDA)(THF)₂} (**CON**⁻)] [111], the external six-membered ring of coronene is engaged in an asymmetric metal ion binding. In contrast, the [{Rb*(18-crown-6)}(**CON**⁻)] complex characterized in our group shows the metal ion coordination to the central ring of **CON**⁻ (Fig. 2b) [110]. The metal-to-centroid distance (3.368(9) Å) is noticeably longer compared to the **Rb-TP**⁻ complex (3.116(3) Å), which is indicative of weaker cation— π interactions. The DFT calculations provided insights into the formation of a hub-bound complex by revealing the existence of multiple C–H··· π interactions

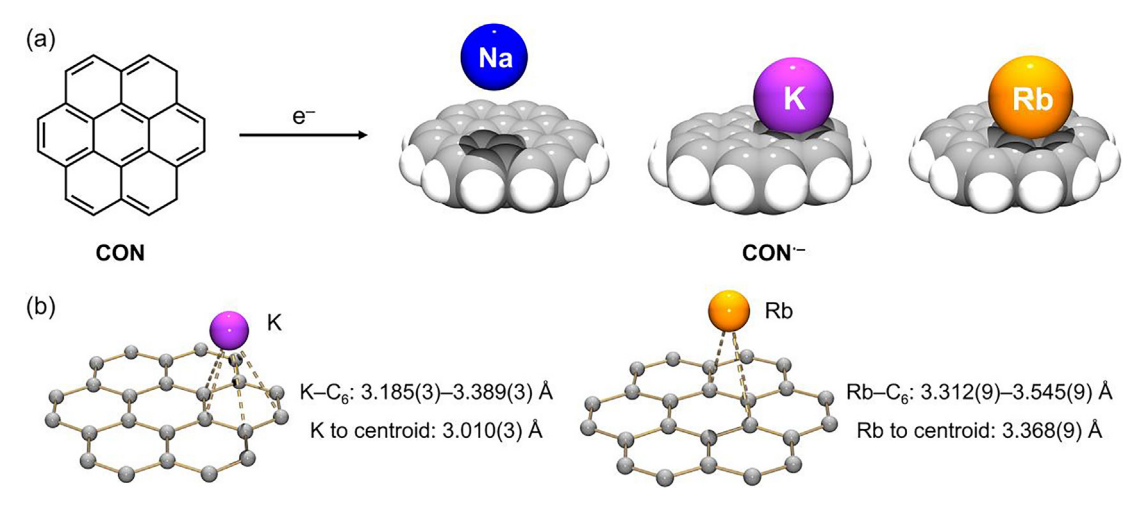


Fig. 2. (a) Chemical reduction of CON to afford the radical-anions, (b) coordination of CON⁻ with K⁺ and Rb⁺ ions.

between the crown ether and the **CON**⁻ surface. These interactions support perfect alignment of two moieties with opposite charges but closely matching sizes, the {Rb⁺(18-crown-6)} cation and the disk-shaped **CON**⁻ anion. The DFT calculations also indicated that the spin density is delocalized over the π -surface, fully supporting the formation of **CON**⁻ radical and the closed-shell Rb⁺ cation in this complex.

In general, interactions of alkali metal ions with planar π -systems are weak and can be affected by a variety of secondary factors. For example, the size and substitution variations built into the structures of crown ethers, which are often used as secondary ligands during crystallization processes, enable fine tuning of metal coordination in the resulting products [112].

These studies were expanded to large nanographene fragments such as hexa-peri-hexabenzocoronenes (HBCs), namely HBC ($C_{42}H_{18}$) and tBu-HBC ($C_{66}H_{66}$), which feature planar geometry and high molecular symmetry (D_{6n}). In contrast to coronene, HBCs show very rich redox properties. The reduction study of HBC carried out by Müllen group using potassium metal showed that this hydrocarbon is capable of accepting up to six electrons [113]. Moreover, $in\ situ\ EPR$ and kinetic UV-vis absorption spectroscopy confirmed the existence of triradical species with the quartet ground state in solution. However, none of the reduced HBC products was isolated in the solid state, and thus no details on alkali metal coordination were known. Only one stable radical-cation of tBu-HBC prepared via electrochemical oxidation was structurally characterized in 2000 [114].

Recently, the triradical trianions of the unsubstituted **HBC** and its *t*Bu-functionalized derivative were isolated with potassium counterions (Fig. 3a) [115]. The products were prepared as purephase crystalline materials that are relatively stable under inert atmosphere conditions, enabling their first single-crystal and powder X-ray diffraction investigation along with magnetic measurements. The crystallographic study revealed the formation of π -complexes of the same composition, [K*(18-crown-6)(THF)₂] [{K*(18-crown-6)}₂(**HBC**^{3.-})] and [K*(18-crown-6)(THF)₂][{K*(18-crown-6)}₂(**tBu-HBC**^{3.-})]. In both, the triply-reduced **HBC** anions have two K* ions coordinated, while one counterion remains solvent-separated. Specifically, the central six-membered ring of the large **HBC** core serves as the alkali metal coordination site (Fig. 3b).

The presence of bulky tBu-substituents affects the metal coordination as reflected by the drastic change of a tilt angle between the cationic moieties and the **HBC** plane from 17.0° to 90.0°. This results in more symmetric coordination of the K⁺ center in the tBu-HBC complex with a notably shorter distance to the ring centroid (2.986(2) Å vs. 3.023(7) Å). Importantly, the magnetic measurements support the existence of a well-isolated S = 3/2 ground state for the triradical of tBu-HBC in the solid state, suggesting such species can be used as building blocks for molecule-based magnets. Further studies of binding preferences of other alkali metals with the highly-reduced HBCs should enable access to multi-spin-bearing nanographenes for emerging single-molecule spintronics and quantum computing nanotechnologies [116–119].

Interestingly, adding electrons to planar nanographene fragments leads to different structural deformations of the PAH core (Table 1). The smaller and less conjugated TP is only slightly distorted in its neutral state (1.8°) but becomes more twisted (6.9°) and curved (5.1°) in the mono-reduced state in the sodium(I) product. This effect is smaller in $[\{K_2^+(DME)\}(TP^-)_2]$ due to the dual metal coordination to the π -surface [99] but becomes more pronounced in π -complexes with a single metal coordination site [100]. Notably, the **TP** core in the potassium(I) complex is severely perturbed (17.6°), but this distortion is reduced upon the metal ion size increase (8.9°). On the contrary, the core distortion in larger planar PAHs is less evident. For instance, an addition of three electrons to **HBCs** results in the torsion angle increase by 9.8° and 5.1° and an added twist of the molecular edges. In comparison, the geometry changes are much smaller in the mono-reduced **CON** (3.2-4.3°); however, this may change with further build-up of negative charge.

3. Adding curvature: Bowl-shaped π -ligands

Bowl-shaped polycyclic aromatic hydrocarbons, also referred to as fullerene fragments, buckybowls or π -bowls, have two distinctly different faces, convex (exo) and concave (endo), both open and available for coordination. This makes carbon bowls a unique class of non-planar π -ligands which are very attractive for metal coordination studies [120–122]. A variety of bowl-shaped PAHs with different dimensions, symmetry, and bowl depth became available in recent years [4,6,123–125], but their coordination chemistry was mainly centered on the smallest corannulene ($C_{20}H_{10}$, C_{5v} , **COR**).

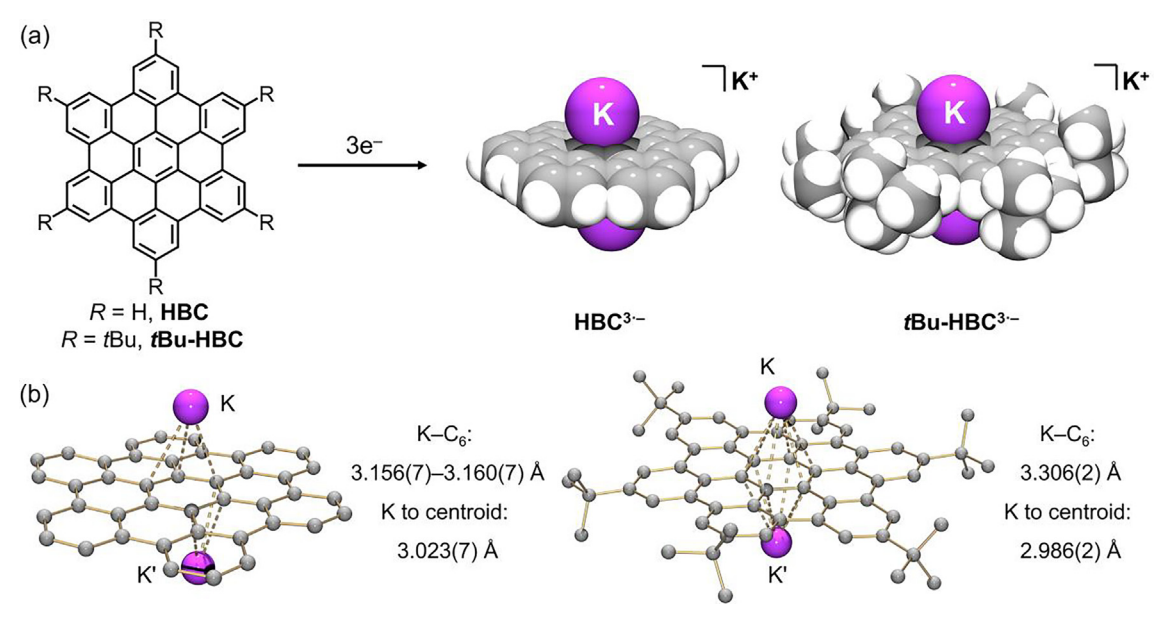
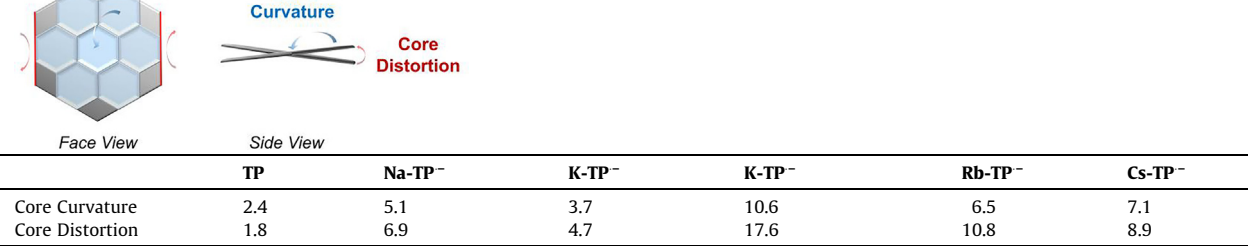


Fig. 3. (a) Chemical reduction of HBCs to afford the triradical-anions, (b) coordination of HBC³⁻ and tBu-HBC³⁻ with K⁺ ions.

Table 1Core curvature and core distortion (°) in negatively-charged **TP**, **CON**, and **HBC**s vs. their neutral parents.

Core



	IP	Na-IP	K-IP	K-1P	KD-1P	CS-IP	Kei.
Core Curvature	2.4	5.1	3.7	10.6	6.5	7.1	[99,100]
Core Distortion	1.8	6.9	4.7	17.6	10.8	8.9	
	CON	Na-CON	K-CON	Rb-CON-			Ref.
Core Curvature	0.4	2.8	1.4	1.6			[110]
Core Distortion	0	3.2	4.3	3.2			
	НВС	K ₃ -HBC ^{3.−}	tBu-HBC	K ₃ -tBu-HBC ³⁻			Ref.
Core Curvature	1.5	4.7	7.6	3.7			[115]
Core Distortion	0	9.8	3.0	8.1			

Note: Core curvature is evaluated by largest dihedral angle between the central and external six-membered rings (blue arrow), and core distortion is measured by largest torsion angle between two parallel edges (red arrow).

The highly-symmetric COR was broadly investigated as a model bowl-shaped ligand to show a range of coordination modes that depend on the metal and its secondary ligand environment [112]. Furthermore, the pioneering works by Scott and Rabinovitz revealed a very rich redox chemistry of **COR** using in situ spectroscopic techniques for product characterization [126-128]. Importantly, COR can accept up to four electrons in stepwise reduction reactions to form a set of bowl-shaped carbanions with gradually increasing negative charges. Using chemical reduction with Group I metals, the successful isolation and crystallographic characterization of all four reduced states of COR were accomplished, revealing its remarkable charge-dependent versatility in alkali metal binding. Notably, the mono- and doubly-reduced COR anions could be isolated in their naked or complexed forms [112], but upon addition of three or four electrons, COR spontaneously selfassembles with multiple alkali metal ions to form unique sandwich-type supramolecular assemblies [129].

For the mono-reduced **COR**⁻⁻ anion, a striking site selectivity in coordination based on the alkali metal ion was demonstrated using X-ray crystallography (Fig. 4a). A comparison of potassium (1.38 Å, [130]), rubidium (1.52 Å), and cesium (1.67 Å) ions revealed their different binding preferences in otherwise similar complexes, $[M^{+}(18\text{-crown-6})(\mathbf{COR}^{-})]$ [131]. The smaller K^{+} and Rb^{+} ions exhibit an exo-binding with relatively weak cation... π interactions to the six-membered ring of the monoanion (K- C_{exo} : 3.142(2)-3.289 (2) Å, Rb- C_{exo} : 3.266(8)-3.479(3) Å) (Fig. 4b), while the large Cs⁺ ion prefers symmetrical endo-coordination to the central fivemembered ring of the bowl (Cs- C_{endo} : 3.423(3)–3.628(3) Å). Theoretical study reaffirmed that the concave placement is favored for a Cs⁺ ion only, while all other alkali metals prefer the convex binding to the **COR**⁻⁻ bowl. The selective concave coordination of Cs⁺ inside the mono- and doubly-reduced corannulene, as well as its rimfunctionalized derivatives, namely monomethylcorannulene $(C_{21}H_{12}, MCOR)$ and pentamethylcorannulene $(C_{25}H_{20}, PMCOR)$,

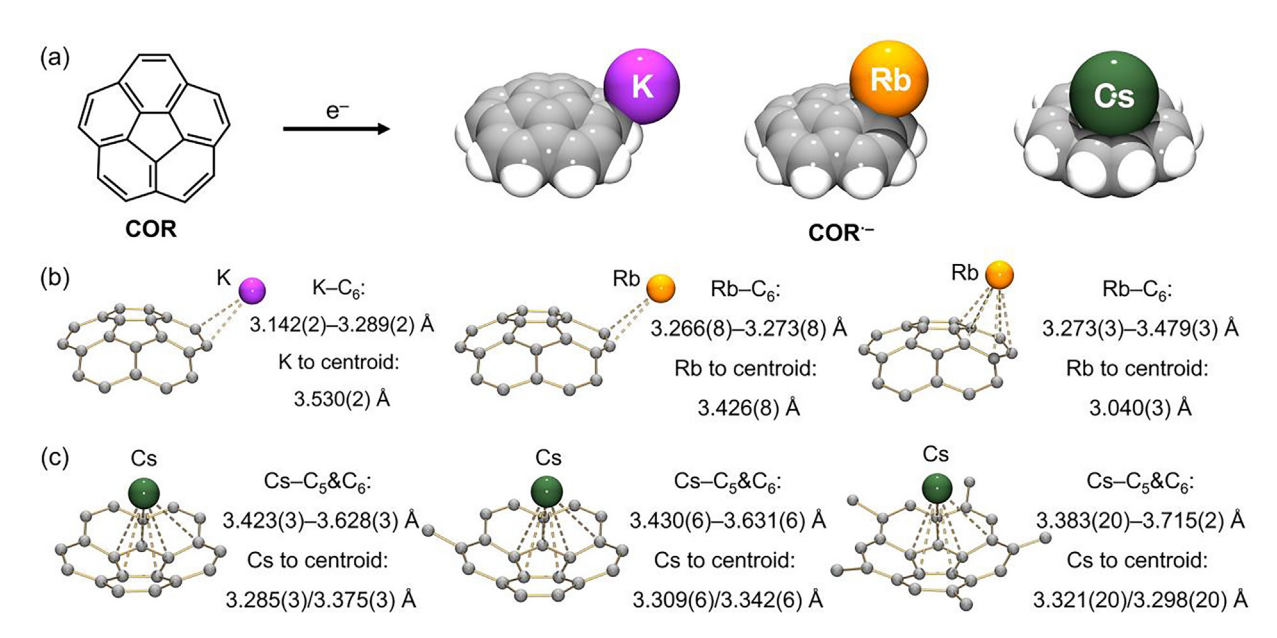


Fig. 4. (a) Chemical reduction of **COR** to afford the radical-anions, (b) coordination of **COR**⁻ with K⁺ and Rb⁺ ions, (c) concave cesium(l) complexes of **COR**⁻, **MCOR**⁻ and **PMCOR**⁻.

was later confirmed in several π -complexes (Fig. 4c) [132,133]. This preference stems from an almost ideal size match of the cesium cation and the *endo* cavity of **COR**⁻ bowl that allows to maximize the electrostatic interactions in these systems.

The doubly-reduced **COR** further reaffirms the above coordination preferences and shows a variety of binding modes that are alkali-metal dependent (Fig. 5a). For example, small Li⁺ and Na⁺ ions favor a convex-only coordination to the **COR**²⁻ core but with notable variations (Fig. 5b top). While the smallest Li⁺ ions show unique double-convex coordination (Li–C_{exo}: 2.313(7)–2.814(8) Å), only one Na⁺ ion could bind to the *exo*-face of **COR**²⁻ (Na–C_{exo}: 2.717(4)–2.996(4) Å). In contrast, larger K⁺ and Cs⁺ ions exhibit both concave and convex coordination at the opposite faces of the bowl (Fig. 5b bottom). In particular, the *endo*-coordinated K⁺ ion is typically bound to the edge (K–C_{endo}: 3.068(4)–3.43(2) Å), while Cs⁺ exhibits symmetrical *endo*- (Cs–C_{endo}: 3.317(12)–3.503 (7) Å) and *exo*-coordination (Cs–C_{exo}: 3.233(9)–3.608(9) Å) to the central five-membered ring of the bowl.

Moving to the triply-reduced corannulene opens new supramolecular chemistry of the highly negatively-charged carbon bowls. The **COR**^{3,-} anions spontaneously self-assemble with multiple alkali metal ions to form a unique sandwich architecture (Fig. 6a) and are not yet known in any other form. An asymmetrical convex-to-convex sandwich with four entrapped Cs⁺ ions is formed with a large deck-to-deck separation of 4.952(5) Å [134]. A similar sandwich structure with four K⁺ ions has a shorter deck-to-deck separation of 4.427(5) Å [135]. Remarkably, the intramolecular magnetic coupling of **COR**^{3,-} radicals in these sandwiches can be fine-tuned by replacing the large intercalated cesium ions with smaller alkali metals [135].

The four-fold chemical reduction of corannulene with lithium metal generates a very electron-rich \mathbf{COR}^{4-} anion with 0.2ê per carbon atom. The single-crystal X-ray diffraction study resolved the long-standing puzzle regarding the structure of this unique product [127] and confirmed that \mathbf{COR}^{4-} self-assembles with five Li⁺ ions sandwiched between the negatively-charged decks to form the $\mathbf{COR}^{4-}/5\mathrm{Li}^+/\mathbf{COR}^{4-}$ dimer (Fig. 6b) [136]. The five encapsulated Li⁺ ions are bound to the six-membered rings of the two

tetra-reduced bowls in the convex-to-convex arrangement (Li- C_{exo} : 2.226(3)–2.718(3) Å). Interestingly, the triple-decker sandwich with a pentanuclear lithium core can exist in different external environments [137], including a highly symmetric (D_{5h}) "naked" sandwich with a deck-to-deck separation of 3.504(5) Å. This structural evidence of the formation of high-nuclearity lithium units held together by bowl-shaped carbanions established a new paradigm for lithium intercalation in curved carbon-based hosts with in-built cavities and pockets.

Furthermore, the synergistic use of dual combinations of Li with K, Rb, or Cs metals in the four-fold reduction of **COR** enabled the formation of unprecedented heterobimetallic sandwich self-assemblies [138–140]. Specifically, the **COR**^{4–} anions are able to keep the highly-charged hexanuclear units of the type $\text{Li}_3\text{M}_3^{6+}$ or LiM_3^{6+} (M = K, Rb, Cs) between two curved π -decks (Fig. 6c,d), thus showing the record alkali metal intercalation limits unmatched by other PAHs. More details on the formation and structures of these remarkable supramolecules can be found in the review [129].

Considering larger carbon bowls, although unique self-assembly pathways of highly-charged carbanions could be expected [141–143], their supramolecular chemistry is yet to be expanded beyond the smallest corannulene [144]. However, original trends in metal binding found for the mono- and doubly-reduced **COR** triggered the exploration of bowl-shaped ligands with different π -framework topologies and atomically-precise doping (vide infra).

The unique selectivity in concave coordination was further reaffirmed by the controlled deprotonation of a deeper bowl, **sumanene** ($C_{21}H_{12}$, C_{3v} , **SUM**, Fig. 7a), using Na and Cs metals having a significant ion size mismatch and different binding preferences [145]. The product exhibited an unprecedented double-concave encapsulation of a large cesium ion by two bowl-shaped sumanenyl anions in $Cs(C_{21}H_{11}^-)_2$ ($Cs-C_{endo}$: 3.254(12)-3.471(12) Å), crystallized with a solvent-separated sodium counterion (Fig. 7b). The revealed cooperativity of two alkali metals in controlled deprotonation and selective coordination by bowl-shaped π -ligands opens new synthetic pathways for preparation of novel heterometallic supramolecules.

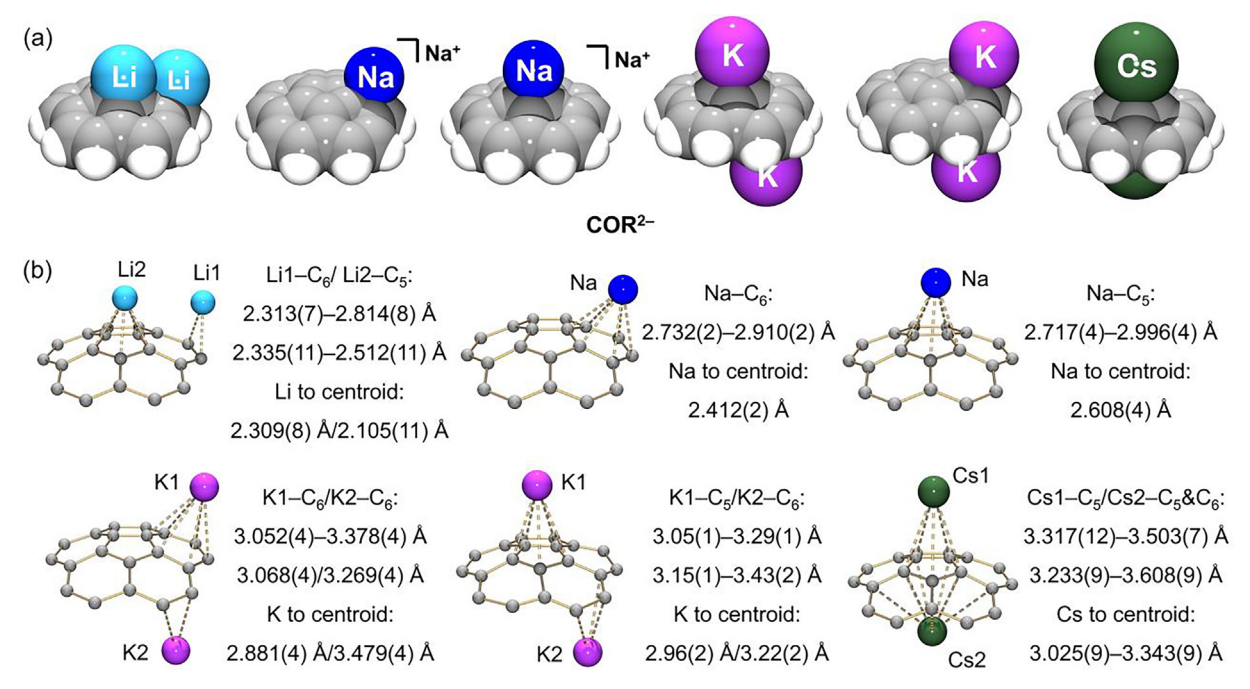


Fig. 5. (a) The doubly-reduced COR²⁻ in different coordination environments, (b) coordination of COR²⁻ with Li⁺, Na⁺, K⁺, and Cs⁺ ions.

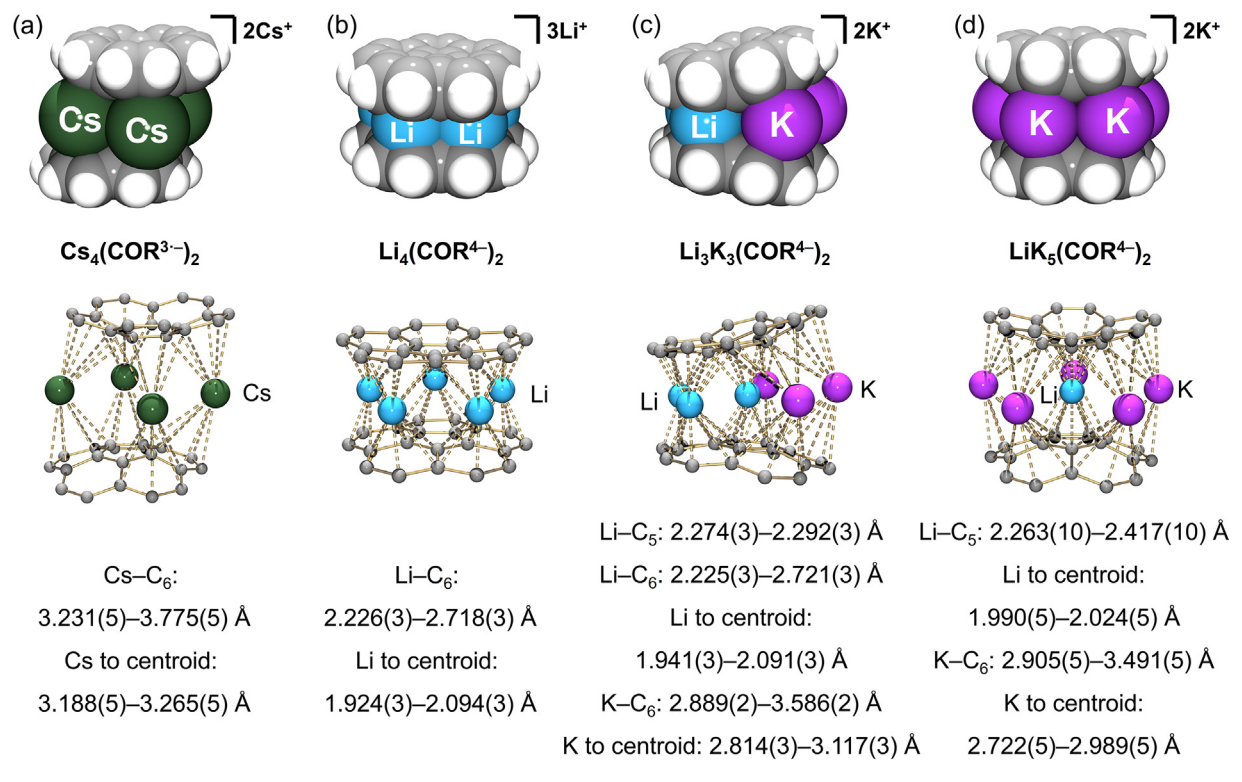


Fig. 6. Encapsulation of alkali metal ions in sandwich-type assemblies (a) Cs₄(COR³⁻)₂, (b) Li₅(COR⁴⁻)₂, (c) Li₃K₃(COR⁴⁻)₂, and (d) LiK₅(COR⁴⁻)₂.

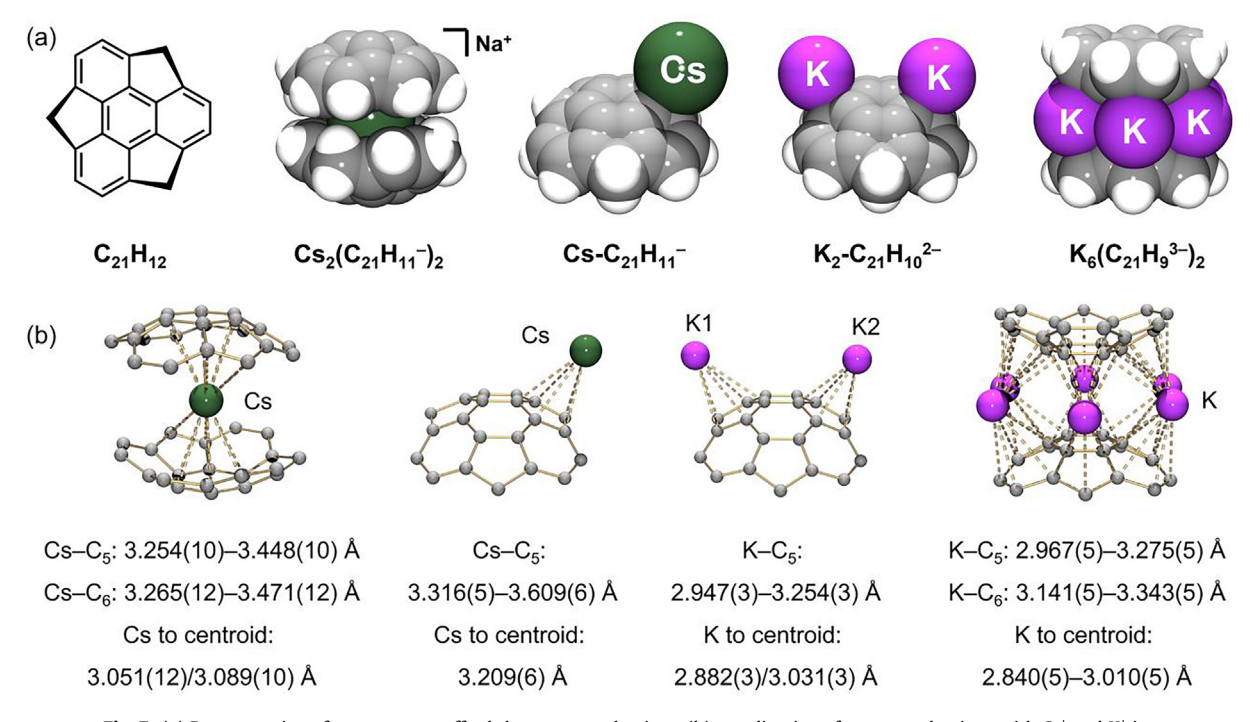


Fig. 7. (a) Deprotonation of sumanene to afford the sumanenyl anions, (b) coordination of sumanenyl anions with Cs⁺ and K⁺ ions.

With the help of theoretical modeling, the stability of the double-concave cesium sandwich was related to stronger cesium cation... π interactions with the sumanenyl bowl compared to weaker interactions with the secondary (THF and 18-crown-6) ligands. This could further expand the toolbox of synthetic chemists as secondary ligands can be deliberately utilized for tuning

metal coordination. For example, with the assistance of more flexible dicyclohexano-18-crown-6 ether, a coordination switch to convex cesium(I) binding to a sumanenyl bowl was induced in the [{Cs*(dc-18-crown-6)}($C_{21}H_{11}^{-}$)] complex [146]. The in-depth theoretical investigation showed that the addition of nonrigid cycloxehyl groups to the 18-crown-6 core enabled multiple

C–H··· π interactions between the cationic {Cs⁺(dc-18-crown-6)} moiety and the convex face of the sumanenyl bowl which resulted in the assisted *exo*-coordination in this unique case.

Additionally, the controlled formation of sumanenyl dianion in the presence of different secondary ligands has allowed the on/off switch of metal binding with K^+ counterions [147]. Particularly, the use of 18-crown-6 ether leads to the formation of a double *exo*-coordinated complex, [$\{K^+(18-crown-6)\}_2(C_{21}H_{10}^{2-1})\}$], with the selective binding of K^+ ions to the two deprotonated five-membered rings ($K-C_{exo}$: 2.947(3)–3.254(3) Å) of the sumanenyl dianion. Further deprotonation of **SUM** with K metal results in the formation of a remarkable mixed-valent aggregate, [$K_7^+(C_{21}H_{10}^{2-1})_2(C_{21}H_9^{3-1})$], in which six K^+ ions encapsulated by two sumanenyl trianions form a highly symmetric (D_{3d}) double-convex sandwich with a deck-to-deck separation of 3.668 Å [144].

Moving to a larger π -bowl with two five-membered rings, **inda**cenopicene (C₂₆H₁₂, IDP, Fig. 8a), results in change of geometry, symmetry, electronic structure, and reactivity [148]. In contrast to COR, IDP was predicted to readily accept up to two electrons only. The accessibility of the mono- and doubly-reduced states was then confirmed by electrochemical and chemical reduction [149]. Two products of the doubly-reduced anion with heavy alkali metals, Rb and Cs, were crystallographically characterized to show the formation of the tetrameric complex and 1D polymer, respectively (Fig. 8b). In the tetramer, the {Rb₂⁺(18-crown-6)} dication occupies the concave cavity formed by two doubly-reduced IDP bowls. These internal rubidium ions bind asymmetrically to the endo surface of IDP²⁻ with the Rb-C distances to the centroids of the fiveand six-membered rings of 2.962(4) and 3.025(4) Å, respectively. In addition, two Rb⁺ ions are externally bound to the five-membered rings on the convex face of the bowls (Rb-C: 3.142(4)-3.382(4) Å), thus forming a discrete organometallic tetramer. The internal binding of a large {Cs $_{-}^{2}$ (18-crown-6)} dication is similar but with notably longer Cs $_{-}$ C distances of 3.282(13) and 3.308(12) Å to the centroids of five- and six-membered rings. In contrast, the external coordination of Cs $_{-}^{+}$ ions to the convex face of \mathbf{IDP}^{2-} enables an extended chain propagation in this product (Fig. 8c). These examples clearly illustrate the effect of ion size increase on the crystal structure type change of the resulting products.

The first investigation of the reduction limits of an interesting PAH having a planar group fused to a corannulene bowl, namely naphtho[2,3-a]corannulene (C₂₈H₁₄, NPCOR, Fig. 9a), and its direct comparison with parent corannulene was accomplished using a combination of theoretical and experimental tools [150]. Both calculations and electrochemistry indicated that the HOMO-LUMO gap of NPCOR is reduced compared to COR, making it a better acceptor than **COR**. The cyclic voltammetry (CV) measurements demonstrated the accessibility and stability of the first and second reduction states, and both were prepared using chemical reduction with Group I metals. The corresponding products of the mono- and doubly-reduced NPCOR were crystallized in their "naked" form with smaller Na⁺ counterions. In contrast, the larger Rb⁺ ions form a π -complex with the dianion of the $[\{Rb^{\dagger}(18\text{-crown-6})\}_{2}]$ (**NPCOR**²⁻)] composition. Specifically, one Rb⁺ ion binds the sixmembered ring of the corannulene bowl in a convex fashion (Rb- C_{exo} : 3.187(6)-3.411(7) Å), while the second one coordinates to the planar naphtho-group from the opposite direction (Rb $-C_{endo}$: 3.191(6)-3.659(6) Å, Fig. 9b). According to the DFT computational study, the observed changes in aromaticity and charge distribution from stepwise electron acquisition are fully consistent with the structural data and metal coordination sites. Interestingly, the direct metal complexation increases the core curvature as the bowl in the rubidium(I) complex (0.857(11) Å) is deeper than that in the neutral parent (0.813(7) Å) and the "naked" dianion (0.794(2) Å).

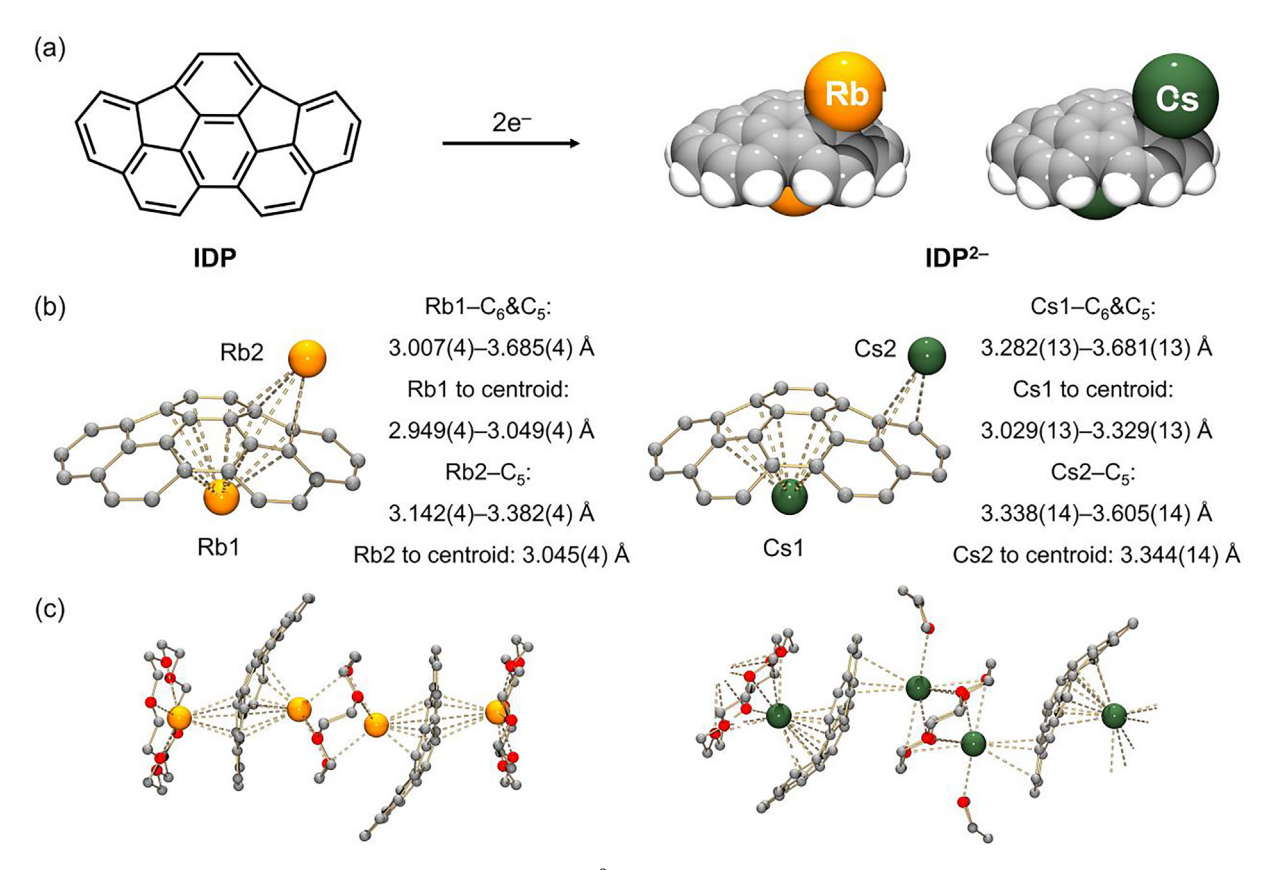


Fig. 8. (a) Chemical reduction of IDP to afford its dianion, (b) coordination of IDP²⁻ with Rb⁺ and Cs⁺ ions, (c) tetrameric rubidium(I) complex, $[\{Rb_2^{+}(18-crown-6)_{1.5}(C_{26}H_{12}^{2})]_{2c}$, and a fragment of the 1D chain in $[\{Cs_2^{+}(18-crown-6)_{2}(THF)(C_{26}H_{12}^{2})]_{2c}$.

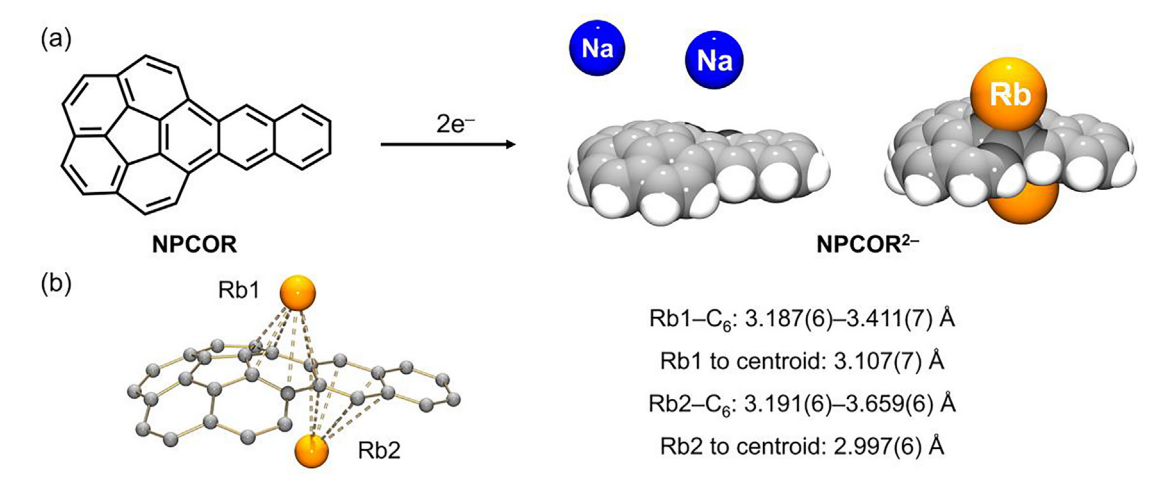


Fig. 9. (a) Chemical reduction of NPCOR to afford its dianions, (b) coordination of NPCOR²⁻ with Rb⁺ ions.

Only recently, studies of the reduction and coordination chemistry of bowl-shaped polyarenes moved to investigation of the heteroatom-containing or atomically-doped buckybowls, including azapentabenzocorannulene and bisdibenzocorannulene [151,152]. Under controlled reaction conditions, the first chemical reduction of an N-doped bowl, tBu-azapentabenzo[bc,ef,hi,kl,no] corannulene (C₃₈H₂₃N, tBu-ACOR, Fig. 10a), was accomplished to afford its mono- and doubly-reduced anions with sodium and cesium metals. As expected, the use of sodium facilitated the formation of the "naked" dianion, while the stepwise reduction of tBu-ACOR with cesium metal allowed the isolation of the monoand doubly-reduced anions complexed with cesium(I) ions as $[{Cs}^{+}(18\text{-crown-6})](tBu-ACOR^{-})]$ and $[{Cs}^{+}(18\text{-crown-6})]_{2}(tBu-ACOR^{-})]_{3}(tBu-ACOR^{-})$ **ACOR**²⁻)]. The former complex shows selective *endo-*coordination of Cs⁺ inside the π -bowl (Cs–C_{endo}: 3.502(3)-3.707(3) Å). In the latter, two Cs+ ions are bound to the concave and convex bowl faces with a wide range of Cs-C distances (Fig. 10b). This first structural analysis of the consequences of the two-step reduction for heteroatom-containing carbon bowls could open new perspectives for the chemistry and applications of atomically-doped non-planar nanographenes. Interestingly, according to the DFT computational study [152], the LUMO of tBu-ACOR has a doubly degenerate ground state, thus indicating the potential of tBu-ACOR to acquire up to four electrons and to exhibit original charge-dependent coordination chemistry.

Although the stepwise chemical reduction results in authentic structural deformation of bowl-shaped π -ligands, the presence of a corannulene core in most systems enables their direct comparison (Table 2). For the mono- and doubly-reduced **COR**, the gradual decrease of core curvature (bowl depth) upon electron uptake can be clearly seen. The bowl depth remains almost unchanged in all metal complexes of the **COR** monoanion (\sim 0.847 Å). In contrast, **Cs₂-COR**²⁻ has a deeper bowl (0.851 Å) compared to other complexes (\sim 0.766 Å) with only edge metal coordination.

For the highly-charged **COR** anions, the reduction outcomes become more nuanced. A dramatic flattening of the bowl to about 0.298 Å is observed in all-lithium sandwich, $\text{Li}_5(\text{COR}^{4-})_2$. However, the insertion of heavier alkali metals between the tetra-reduced decks results in the significant bowl curvature increase, $\text{Li}_3 \text{K}_5^{6+}$ (0.620 Å), $\text{Li}_3 \text{Rb}_5^{6+}$ (0.705 Å, [140]), $\text{Li}_3 \text{Cs}_5^{6+}$ (0.860 Å, [139]), and LiK_5^{6+} (0.860 Å). Similarly, a bowl depth increase is observed when replacing potassium cations (0.808 Å) with cesium (0.850 Å) in the sandwich architectures formed by the triply-reduced COR^{3-} bowls.

Compared to **COR** anions, the bowl depth change of **SUM** during stepwise deprotonation is less distinctive, with a slight increase from 1.114 Å in neutral to 1.210 Å in the triply-charged state. In

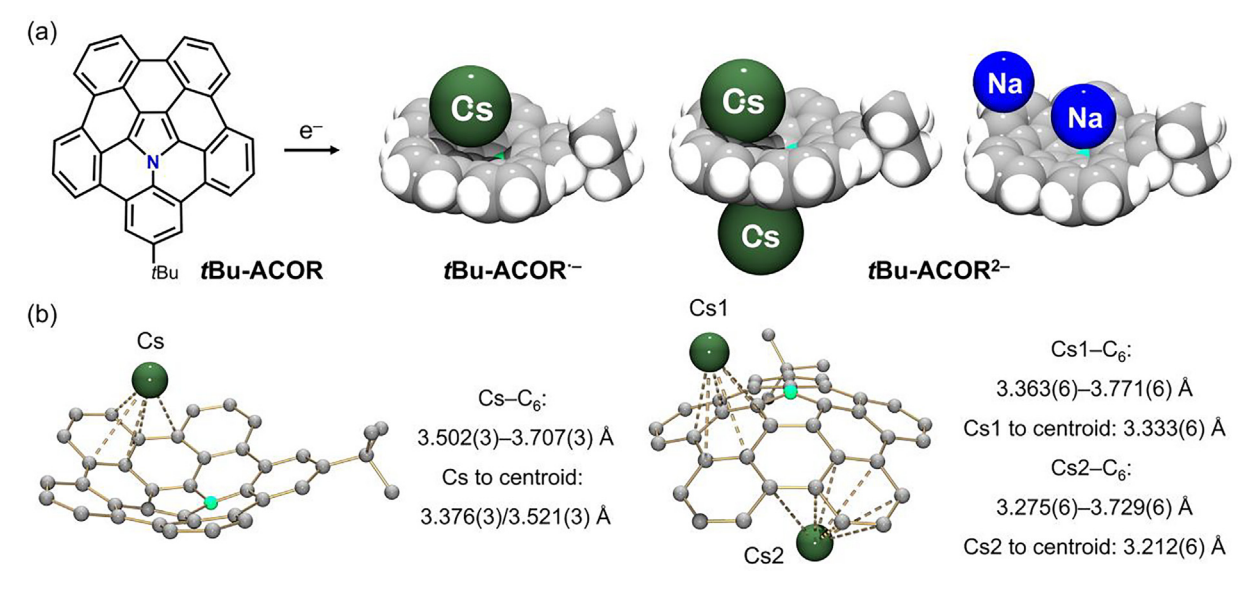


Fig. 10. (a) Chemical reduction of tBu-ACOR to afford its anions, (b) coordination of tBu-ACOR⁻ and tBu-ACOR²⁻ with Cs⁺ ions.

Table 2
Core curvature (Å) and core distortion (°) in negatively-charged COR, SUM, IDP, NPCOR, and tBu-ACOR vs. their neutral parents.

	COR	K-COR	Rb-COR	Cs-COR		Ref.
Core Curvature	0.875	0.846	0.834/0.862	0.846		[131,153]
Core Distortion	2.1	1.9	4.5/1.7	2.7		
	Li ₂ -COR ²⁻	Na ₂ -COR ²⁻	K ₂ -COR ²⁻	Cs ₂ -COR ²⁻		Ref.
Core Curvature	0.796	0.795/0.799	0.785/0.655	0.851		[132,153,154]
Core Distortion	1.0	0.9/1.2	2.7/6.4	3.2		
	K ₄ (COR ³) ₂	Cs ₄ (COR ³) ₂				Ref.
Core Curvature	0.808	0.850				[134,135]
Core Distortion	1.8	3.1				
	Li ₅ (COR ⁴⁻) ₂	$Li_3K_3(COR^{4-})_2$	$Li_3Rb_3(COR^{4-})_2$	Li ₃ Cs ₃ (COR ⁴⁻) ₂	LiK ₅ (COR ⁴⁻) ₂	Ref.
Core Curvature	0.288/0.307	0.620	0.703/0.706	0.741/0.766	0.860	[136,138-140]
Core Distortion	1.7	3.5	1.5	4.2	2.3	
	$C_{21}H_{12}$	$Cs(C_{21}H_{11}^-)_2$	Cs-C ₂₁ H ₁₁	K_2 - $C_{21}H_{10}^{2-}$	$K_6(C_{21}H_9^{3-})_2$	Ref.
Core Curvature	1.114	1.214	1.147	1.154	1.210	[144-147]
Core Distortion	0	2.7	4.0	2.1	0.4	
	IDP	Rb ₂ -IDP ²⁻	Cs ₂ -IDP ²⁻			Ref.
Core Curvature	0.925	0.933	0.976			[149]
Core Distortion	1.6	1.9	4.9			
	NPCOR	Na ₂ -NPCOR ²⁻	Rb ₂ -NPCOR ²⁻			Ref.
Core Curvature	0.813	0.794	0.857			[150]
Core Distortion	3.3	4.9	3.7			
	tBu-ACOR	Na ₂ -tBu-ACOR ²⁻	Cs-tBu-ACOR -	Cs ₂ -tBu-ACOR ²⁻		Ref.
Core Curvature	0.871	0.887	0.897	0.908		[151]
Core Distortion	1.2	3.3	3.1	2.7		-

Note: Core curvature is illustrated by bowl depth from the bowl bottom to the bowl edge, and core distortion is measured by the largest torsion angle between two parallel edges of the bowl core.

the π -expanded **IDP** bowl, the rubidium ion coordination leads to a slight increase of the core curvature (0.933 Å), which is further enhanced by the heavier cesium ion (0.976 Å). Similar to **COR**, a curvature decrease is observed in the naked **NPCOR**²⁻ anion (0.794 Å). On the contrary, the asymmetrical double-side metal binding allows the formation of a noticeably deeper bowl (0.857 Å) in the rubidium complex of **NPCOR**²⁻. Interestingly, in the series of larger N-doped **tBu-ACOR**, the surface extension confines the bowl shape during chemical reduction. Instead of flattening, the inner corannulene core in **tBu-ACOR** becomes more curved upon stepwise electron addition (0.887 Å), which is more pronounced in the presence of the coordinated Cs⁺ ions (0.897 and 0.908 Å). Although the effect of reduction and metal coordination are clearly reflected in the curvature changes, other core distortions are less pronounced for carbon bowls (Table 2).

The literature analysis shows that only for the smallest corannulene systematic investigation of the charge, ion size, and solvent media was carried out to reveal unique trends in alkali metal coordination [137,155]. While the proven ability of selected carbon bowls to undergo reversible multi-electron reduction and alkali metal intercalation makes them very attractive targets for energy storage applications, these studies are yet to be expanded to larger bowl-shaped π -systems. Further discussion of the effect of surface size, symmetry, doping and charge of the nanocarbon bowls on their metal coordination and self-assembly trends remains open [156].

4. Bent and twisted molecular nanographenes

The design bottom-up synthesis of molecular nanographenes (NGs) provided access to a variety of novel carbon architectures

with controlled compositions and dimensions [157-165]. Driven by their unique non-planar structures and interesting properties, the numbers of π -expanded molecular nanographenes built around five-, seven-, and eight-membered rings with positive or negative curvature are rapidly growing in recent years [18,19,24,166–173]. One of the emerging applications includes the use of non-planar carbon-based materials in energy storage and transport [52,54]. This stems from the ability of large **NG**s to reversibly uptake multiple electrons and also to provide the internal cavities for guest encapsulation. The multi-electron acceptor abilities of NGs can be probed in chemical reduction reactions with Group 1 metals. At the same time, structural characterization of the resulting alkalimetal doped products could provide insights into the metal binding sites and structural responses of carbon frameworks to electron addition and metal coordination [152,174]. A better understanding of these effects for molecular NGs should stimulate their material chemistry applications. To illustrate the influence of metal ion size and π -surface topological effects we review herein several interesting crystallographically confirmed examples.

The successful synthesis of π -expanded nanographene having a corannulene bowl fused to a [6]helicene moiety, ($C_{76}H_{64}$, **CBN**), was recently accomplished in Martín group [175]. This chiral hybrid **NG** with positive curvature (highlighted in red, Fig. 11) was probed in the first chemical reduction study with Na metal, which revealed a prompt formation of its doubly-reduced state in solution [176]. The resulting product was crystallized in the presence of 18-crown-6 ether and identified by single-crystal X-ray diffraction as [$\{Na^+(18-crown-6)(THF)\}_2(CBN^{2-})$]. Notably, the product is racemic and contains an equimolar ratio of negatively-charged *P*- and *M*-isomeric molecular nanographenes. In the crystal structure, the two isomers with opposite chirality form a large cylindrical void (1277 ų) defined by in-built curvature of the doubly-

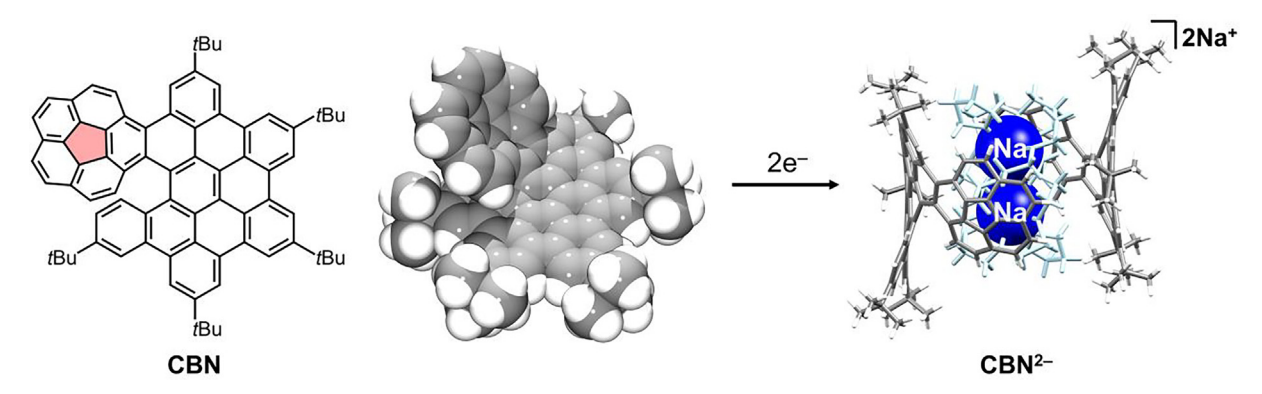


Fig. 11. Structure of CBN and its chemical reduction to afford Na₂-CBN²⁻.

reduced carbanions. This large internal cavity is capable of entrapping guests with complementary size and shape such as a sizable $\{\text{Na}^{\star}(18\text{-crown-6})(\text{THF})\}_2$ dication (960 ų) (Fig. 11) [176]. The resulting host–guest assembly is supported by multiple C–H··· π interactions (2.417(3)–2.743(3) Å) between the complementary cationic and anionic units. Importantly, the doubly-reduced **CBN** can be reversibly oxidized back to the neutral state, indicating the stability and inherent flexibility of its carbon framework towards the redox processes.

In order to promote direct cation··· π interactions, heavy alkali metal congeners have to be utilized in the chemical reduction of nonplanar **NG**s. In this regard, a remarkable warped molecular nanographene ($C_{80}H_{30}$, **WNG**) centered around a five-membered ring (highlighted in red, Fig. 12a) with five seven-membered rings (highlighted in blue) embedded into a hexagonal carbon lattice was reported by Itami group in 2013 [16]. This combination of odd-membered rings resulted in a topologically original double-concave carbon framework. The revealed rich redox properties of **WNG** [16] prompted exploration of the first chemical reduction behavior of this unique nanographene [177]. While multielectron reduction was achieved with several alkali metals in solution, the stepwise reduced products were successfully crystallized

only with large Cs⁺ ions as [Cs⁺(diglyme)₂][WNG⁻⁻], [Cs₂⁺(18-crown- $6)_2(WNG^{2-})$, and $[Cs_2^{\dagger}(18\text{-crown}-6)_3][\{Cs^{\dagger}(18\text{-crown}-6)\}_2(WNG^{3-})]$ -)₂. The calculated 3D molecular electrostatic potential (MEP) maps showed the gradual increase of the negative charge localization on the central part of the WNG framework, thus generating perfect metal binding pockets for accommodation of large cesium cations. Indeed, the Cs⁺ ion was found to directly coordinate to the central corannulene core of the WNG²⁻ anion (Fig. 12b), reinforcing the binding preferences observed in the parent COR [132]. In the crystal structure of the triply-reduced product, two Cs⁺ ions are filling both cavities of a double-concave WNG framework. Specifically, one Cs+ ion binds to the central five-membered ring, while the second Cs+ ion asymmetrically coordinates to the six-membered ring on the opposite side of \mathbf{WNG}^{3-} . The detailed structural analysis coupled with theoretical calculations revealed that WNG surface undergoes subtle swinging distortions which are accompanied by notable changes in the electronic structure and site-dependent aromaticity caused by sequential electron addition. Notably, the successful isolation of three different reduced states of WNG with up to three electrons added to its large π -conjugated system opens new opportunities for practical applications of different NGs in chemical and electrochemical processes.

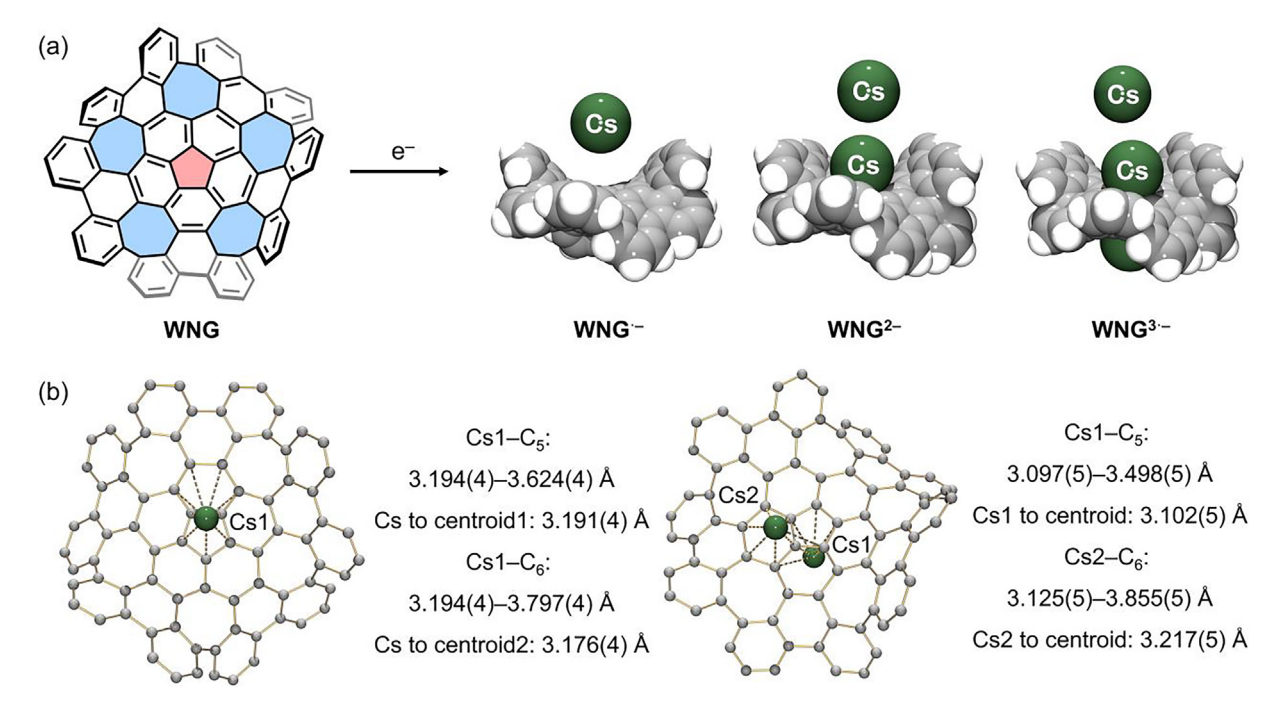


Fig. 12. (a) Stepwise chemical reduction of WNG to afford mono-, doubly-, and triply-reduced states, (b) coordination of WNG²⁻ and WNG³⁻ anions with Cs⁺ ions.

In contrast to an open double-concave **WNG** framework, a large PAH around a central eight-membered octaphenyltetrabenzocyclooctatetraene (C₇₂H₄₈, **OPTBCOT**) exhibits a highly contorted structure with deep pockets and negative curvature (highlighted in blue, Fig. 13a). Moreover, eight phenyl side-rings of **OPTBCOT** contribute to the peripheral structural flexibility needed for host-guest interactions with encapsulated solvent molecules [178,179]. To gain insights into electron accepting properties of **OPTBCOT**, its chemical reduction behavior was probed with lithium metal [179]. The Li-induced reaction resulted in the formation of a remarkable tetraanion of **OPTBCOT** which was stabilized by the coordination of two internally bound Li⁺ ions with two external solvent-separated cations, [{Li(THF)₄}₂{-Li₂(**OPTBCOT**⁴⁻)}] (Fig. 13b). Notably, no examples of such highlyreduced carbanions exist for the parent COT or other smaller COTbased PAHs. The variable-temperature ⁷Li NMR spectroscopy confirmed the presence of three types of Li⁺ ions in solution with clearly different internal binding sites in full agreement with the crystal structure. Specifically, one Li⁺ ion is deeply inserted into the internal pocket of the highly-twisted carbon framework with multiple short Li-C distances of 2.303(9)-2.544(9) Å. The second Li⁺ ion is fully sandwiched by two peripheral phenyl rings of the **OPTBCOT**⁴⁻ anion. The flexibility of these phenyl rings holding one Li⁺ ion is illustrated by a large rotation angle (33.6°) compared to a neutral PAH. This sandwich with a deck-to-deck separation of 3.797(7) Å exhibits slightly asymmetric Li⁺ ion binding with the Li-C distances ranging over 2.261(9)-2.584(9) Å. The discovery of the first tetra-reduced COT-based carbanion was supported by the DFT calculations which revealed significant stabilization through the internal lithium coordination. Importantly, ¹H NMR spectroscopy confirmed that the four-fold reduction of **OPTBCOT** is reversible and the tetraanion can be converted back to the neutral state by exposure to air. This finding illustrates the great potential of the highly contorted π expanded NGs with multi-electron acceptor abilities and reversible lithium-ion uptake for energy storage applications.

A similar connection between rich reduction properties and energy storage applications was recently demonstrated for another negatively curved nanographene (highlighted in blue, Fig. 14a), octabenzo[8]circulene ($C_{64}H_{32}$, **OB8C**), reported by Miao group in 2019 [180]. The ability of **OBSC** to acquire multiple electrons was demonstrated in stepwise reduction reactions with two alkali metals, Li and Na [181]. A remarkable structure of the penta-reduced **OBSC** was confirmed crystallographically, revealing both internal and external alkali metal binding (Fig. 14b). While two sodium(I) ions occupy structural pockets formed by the highly curved core of OB8C5--, the other three sodium(I) ions remain solventseparated from the negatively-charged complexed framework. Specifically, Na1 is capped by two THF molecules and binds to the internal surface of **OB8C**⁵ with the Na–C distances ranging over 2.616(5)-2.855(5) Å. Na2 binds to the opposite side of the pentaanion core (Na-C: 2.560(5)-3.003(5) Å) and has one coordinated THF molecule. Importantly, the designed covalently-linked framework based on the OB8C units showed advanced anode material properties for lithium-ion batteries with a maximum capacity of 830 mAh·g⁻¹ at a current density of 100 mA·g⁻¹ [181].

Chemical reduction leads to marked structural deformation of all π -expanded and twisted **NG** frameworks. Due to their large topological differences, only individual evaluation of their structural response to electron charging can be carried out (Table 3). In **CBN**²⁻ anion, the two-electron addition results in a curvature increase of the HBC core (Δ = 16.3°) accompanied by a large twist of the helicenic unit (Δ = 33.8°), but the curvature of the corannulene bowl is only slightly reduced (Δ = 2.3°). In the series of **WNG** anions, the central corannulene core is flattened from 17.7° in neutral parent to 11.8° in the **WNG**³⁻ anion. In contrast, a noticeably larger curvature observed in **WNG**²⁻ anion (18.1°) can be a consequence of asymmetric Cs⁺ ion binding to one side of the **NG** surface. At the same time, the evaluation of molecular core distortion shows some decrease along the series of **WNG** anions compared to the neutral parent. The core of **OPTBCOT** remains almost

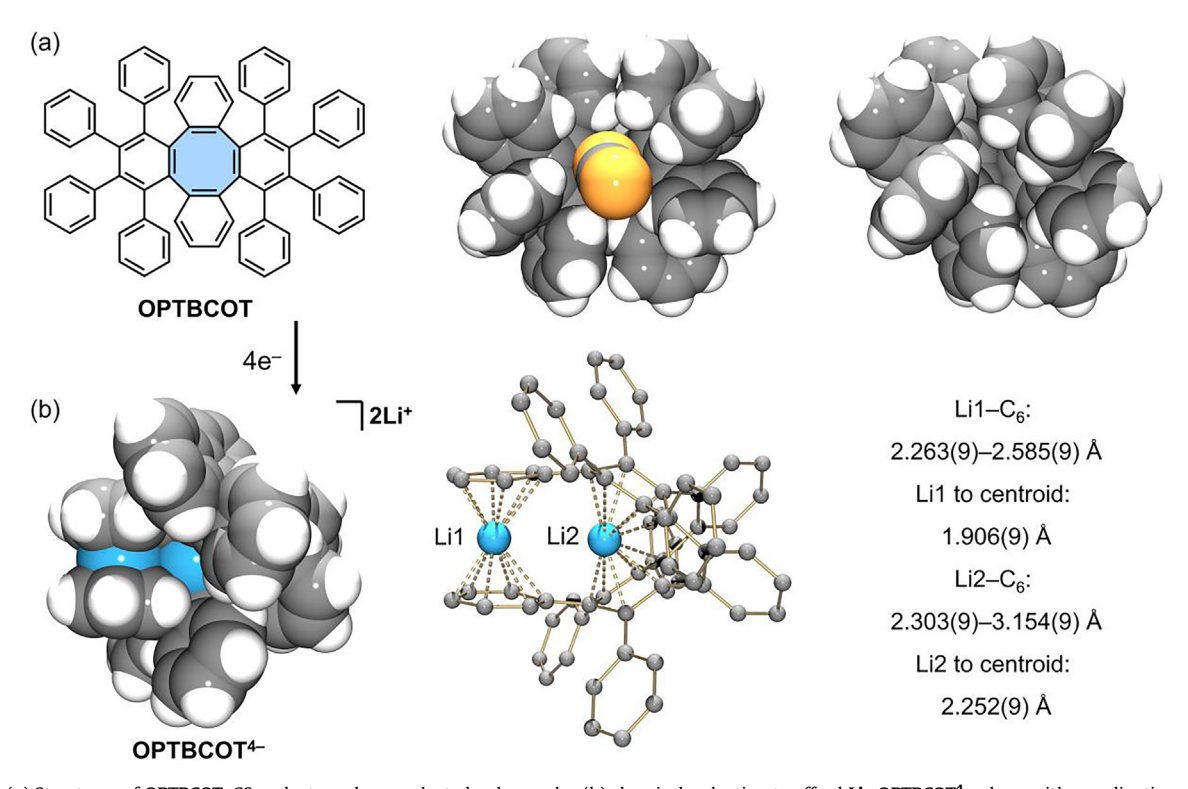


Fig. 13. (a) Structures of OPTBCOT, CS₂-solvate and non-solvated polymorphs, (b) chemical reduction to afford Li₂-OPTBCOT⁴⁻, along with coordination of Li⁺ ions.

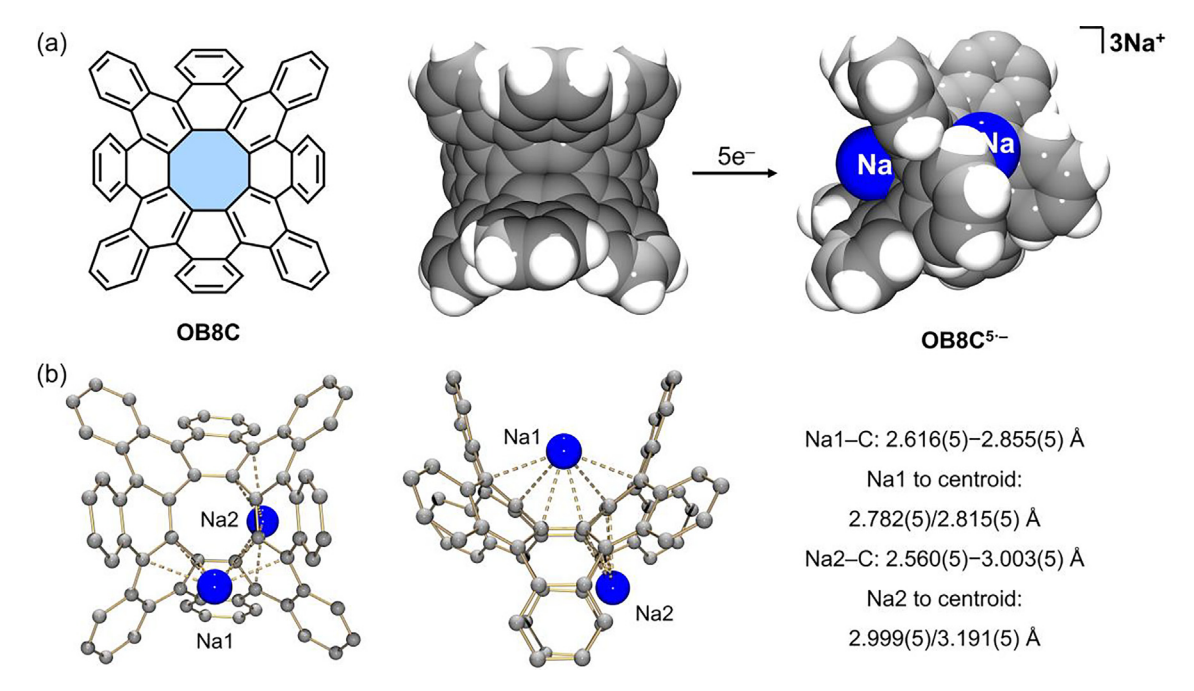


Fig. 14. (a) Chemical reduction of OB8C to afford Na₂-OB8C⁵⁻, (b) coordination of OB8C⁵⁻ with internal Na⁺ ions (two different views).

Table 3
Core curvature and distortion in the negatively-charged CBN, WNG, OPTBCOT, and OB8C vs. their neutral parents.

	CBN	Na ₂ -CBN ²⁻			Ref.
Core Curvature	0.829 Å	0.859 Å			[176]
Core Distortion	47.0°	80.8°			
	WNG	Cs-WNG	Cs ₂ -WNG ²⁻	Cs ₃ -WNG ³	Ref.
Core Curvature	0.316 Å	0.20 Å	0.432 Å	0.170 Å	[177]
Core Distortion	56.2°	50.8°	50.8°	49.4°	
	ОРТВСОТ	Li ₂ -OPTBCOT ⁴⁻			Ref.
Core Curvature	59.5°	62.2°			[179]
Core Distortion	66.7°	33.1°			
	OB8C	Na ₂ -OB8C ⁵			Ref.
Core Curvature	38.4°	40.8°			[181]
Core Distortion	70.8°	74.9°			

Note: For **CBN**, core curvature is reflected by bowl depth of the corannulene unit, and core distortion is measured by twist angle in the helicene unit. For **WNG**, core curvature is calculated by bowl depth of the corannulene unit, and core distortion is evaluated by largest dihedral angle between the central five-membered ring and the peripheral six-membered ring. For **OPTBCOT**, core curvature is evaluated by largest dihedral angle in the tetraphenylene unit, and core distortion is measured by largest dihedral angle between the phenyl ring and the ring of the attachment. For **OBSC**, core curvature is described by largest dihedral angle in the [8] circulene unit, and core distortion is reflected by largest dihedral angle between the external six-membered rings.

unchanged (Δ = 2.7°) upon four-fold reduction, while the peripheral phenyl rings are notably rotated by 33.6° in respect to the central ring to accommodate lithium ion insertion. In comparison, the core curvature and core distortion of the fully conjugated and rigid **OB8C**^{5.–} anion are less evident as shown by small variations of 2.4° and 4.1°, respectively.

In addition to the above **NG**s, the recent investigation of severely twisted helicenes revealed their external alkali metal coordination preferences upon multi-electron reduction [182–184]. A comparison of alkali-metal doped helicenes ranging from a boron-doped double[5]helicene [182] to a double[7]helicene [183] and a bilayer nanographene with a [10]helicene unit [184] shows that their binding sites depend on the framework topology, negative charge, and alkali metals. These first studies start to unlocking coordination chemistry of π -expanded helicenes and need to include encapsulation of the smallest lithium ions.

5. Conclusions

This overview of metal coordination of a diverse set of PAHs upon chemical reduction covers planar, curved, and twisted molecular nanographenes, using the recent crystallographically confirmed examples of alkali metal intercalated products. Their direct comparison reveals the prominent effect of carbon framework topology and shows interesting metal binding trends along with individual structural responses of π -systems to addition of multiple electrons.

For planar graphene fragments, the alkali metal ion coordination depends on the PAH surface size and symmetry and can be modulated with the help of secondary ligands. The electron acquisition leads to notable core distortion, which is more distinct in smaller PAHs like **TP** but less evident in larger systems like **CON** and **HBC**s. For the most representative bowl-shaped PAHs such

as **COR** and **SUM**, the stepwise negative charge build-up, metal ion size, and solvent effects are the most striking. These highlysymmetric carbon bowls show unique metal ion size-dependent face specificity in coordination. A comparison with π -expanded bowls such as IDP, NPCOR, and tBu-ACOR demonstrates their individual metal binding preferences and original geometry perturbation upon two-electron uptake. However, coordination chemistry of large bowl-shaped π -ligands awaits for more studies and discoveries, as systematic investigation of the highly-negatively charged states remains limited to the smallest COR and SUM bowls.

For bent, warped, and twisted molecular nanographenes with multiple internal and external sites chemical reduction opens entirely different coordination chemistry, accompanied by unique site-specific metal intercalation coupled with distinct framework responses. This stems from the ability of large NGs to reversibly uptake multiple electrons and to provide their internal cavities for size-selective guest encapsulation. The revealed multielectron accepting abilities and alkali metal intercalation of molecular NGs should stimulate their future application as advanced functional materials for energy storage and transport. At the same time, the expansion of this discussion to novel contorted nanocarbon systems with original framework topologies, hybrid and multilayered structures should pave the way to new coordination chemistry and a wealth of practical applications.

Credit authorship contribution statement

Zheng Zhou: Formal analysis, Writing. Marina A. Petrukhina: Conceptualizitation, Project administration, Supervision, Funding acquisition, Formal analysis, Writing.

Data availability

All data used have been published in the form of manuscript and supporting information files.

Declaration of Competing Interest

The authors declare that they have no known competing financial interests or personal relationships that could have appeared to influence the work reported in this paper.

Acknowledgements

Financial support of this work from the U. S. National Science Foundation, CHE-2003411, is gratefully acknowledged by M. A. P. We thank Dr. Zheng Wei (UAlbany) for his assistance with X-ray diffraction experiments and ChemMatCARS Sector 15 supported by the National Science Foundation under grant number NSF/ CHE-1834750. This research used resources of the Advanced Photon Source, a U.S. Department of Energy (DOE) Office of Science User Facility operated for the DOE Office of Science by Argonne National Laboratory under Contract No. DE-AC02-06CH11357. M. A. P. is also very grateful to all former group members and collaborators.

References

- [1] H.W. Kroto, J.R. Heath, S.C. O'Brien, R.F. Curl, R.E. Smalley, Nature 318 (1985) 162-163.
- S. Iijima, Nature 354 (1991) 56-58.
- [3] L.T. Scott, Pure Appl. Chem. 68 (1996) 291-300.
- [4] X. Li, F. Kang, M. Inagaki, Small 12 (2016) 3206-3223.
- [5] E.M. Muzammil, D. Halilovic, M.C. Stuparu, Commun. Chem. 2 (2019) 58.
- [6] W. Wang, X. Shao, Org. Biomol. Chem. 19 (2021) 101-122.
- [7] S. Yamago, E. Kayahara, J. Synth. Org. Chem., Jpn. 77 (2019) 1147-1158.
- [8] Q.-H. Guo, Y. Qiu, M.-X. Wang, J.F. Stoddart, Nat. Chem. 13 (2021) 402-419.

- [9] Y. Li, H. Kono, T. Maekawa, Y. Segawa, A. Yagi, K. Itami, Acc. Mater. Res. 2 (2021) 681-691.
- [10] S. Mirzaei, E. Castro, R.H. Sánchez, Chem. Eur. J. 27 (2021) 8642-8655.
- [11] M. Hermann, D. Wassy, B. Esser, Angew. Chem. Int. Ed. 60 (2021) 2-26.
- [12] T. Iwamoto, Y. Watanabe, Y. Sakamoto, T. Suzuki, S. Yamago, J. Am. Chem. Soc. 133 (2011) 8354-8361.
- [13] E.R. Darzi, R. Jasti, Chem. Soc. Rev. 44 (2015) 6401-6410.
- [14] M.R. Golder, R. Jasti, Acc. Chem. Res. 48 (2015) 557-566.
- [15] A. Haupt, D. Lentz, Chem. Eur. J. 25 (2019) 3440-3454.
- [16] K. Kawasumi, Q. Zhang, Y. Segawa, L.T. Scott, K. Itami, Nat. Chem. 5 (2013) 739_744
- [17] S. Ito, Y. Tokimaru, K. Nozaki, Angew. Chem. Int. Ed. 54 (2015) 7256-7260.
- [18] K. Shoyama, F. Wurthner, J. Am. Chem. Soc. 141 (2019) 13008-13012.
- [19] M. Krzeszewski, L. Dobrzycki, A.L. Sobolewski, M.K. Cyranski, D.T. Gryko, Angew. Chem. Int. Ed. 60 (2021) 14998-15005.
- [20] W. Wang, F. Hanindita, Y. Hamamoto, Y. Li, S. Ito, Nat. Commun. 13 (2022) 1498.
- [21] K. Ikemoto, R. Kobayashi, S. Sato, H. Isobe, Angew. Chem. Int. Ed. 56 (2017) 6611-6614
- [22] S.H. Pun, O. Miao, Acc. Chem. Res. 51 (2018) 1630-1642.
- [23] J.M. Fernández-García, P.J. Evans, S. Filippone, M.Á. Herranz, N. Martín, Acc. Chem. Res. 52 (2019) 1565-1574.
- [24] J. Urieta-Mora, M. Krug, W. Alex, J. Perles, I. Fernandez, A. Molina-Ontoria, D. M. Guldi, N. Martin, J. Am. Chem. Soc. 142 (2020) 4162–4172.
- [25] Chaolumen, I.A. Stepek, K.E. Yamada, H. Ito, K. Itami, Angew. Chem. Int. Ed. 60 (2021) 23508-23532.
- [26] K. Itami, G. González Miera, S. Matsubara, H. Kono, K. Murakami, Chem. Sci. 13 (2022) 1848-1868.
- [27] K. Ikemoto, M. Akiyoshi, T. Mio, K. Nishioka, S. Sato, H. Isobe, Angew. Chem. Int. Ed. 61 (2022) e202204035.
- [28] Y. Zhang, S.H. Pun, Q. Miao, Chem. Rev. 122 (2022) 14554-14593.
- [29] S. Cui, G. Zhuang, D. Lu, Q. Huang, H. Jia, Y. Wang, S. Yang, P. Du, Angew. Chem. Int. Ed. 57 (2018) 9330–9335.
- [30] Y. Segawa, M. Kuwayama, Y. Hijikata, M. Fushimi, T. Nishihara, J. Pirillo, J. Shirasaki, N. Kubota, K. Itami, Science 365 (2019) 272-276.
- [31] M. Krzeszewski, H. Ito, K. Itami, J. Am. Chem. Soc. 144 (2021) 862-871.
- [32] W. Fan, T. Matsuno, Y. Han, X. Wang, Q. Zhou, H. Isobe, J. Wu, J. Am. Chem. Soc. 143 (2021) 15924-15929.
- [33] J. Zhu, Y. Han, Y. Ni, S. Wu, Q. Zhang, T. Jiao, Z. Li, J. Wu, J. Am. Chem. Soc. 143 (2021) 14314-14321.
- [34] J.H. May, J.M. Van Raden, R.L. Maust, L.N. Zakharov, R. Jasti, Nat. Chem. 15 (2023) 170-176.
- [35] Z. Sun, K. Ikemoto, T.M. Fukunaga, T. Koretsune, R. Arita, S. Sato, H. Isobe, Science 363 (2019) 151-155.
- [36] J. Wang, X. Zhang, H. Jia, S. Wang, P. Du, Acc. Chem. Res. 54 (2021) 4178-
- [37] Z. Sun, K. Li, Synlett 32 (2021) 1581-1587.
- [38] N.J. Schuster, R. Hernandez Sanchez, D. Bukharina, N.A. Kotov, N. Berova, F. Ng, M.L. Steigerwald, C. Nuckolls, J. Am. Chem. Soc. 140 (2018) 6235–6239.
- [39] P.J. Evans, J. Ouyang, L. Favereau, J. Crassous, I. Fernandez, J. Perles, N. Martin, Angew. Chem. Int. Ed. 57 (2018) 6774-6779.
- [40] Y. Zhu, X. Guo, Y. Li, J. Wang, J. Am. Chem. Soc. 141 (2019) 5511-5517.
- [41] P. Izquierdo-García, J.M. Fernández-García, I. Fernández, J. Perles, N. Martín, J. Am. Chem. Soc. 143 (2021) 11864-11870.
- [42] Y. Chen, C. Lin, Z. Luo, Z. Yin, H. Shi, Y. Zhu, J. Wang, Angew. Chem. Int. Ed. 60 (2021) 7796-7801.
- [43] Y. Zhu, J. Wang, Acc. Chem. Res. 56 (2023) 363-373.
- [44] R.L. Maust, P. Li, B. Shao, S.M. Zeitler, P.B. Sun, H.W. Reid, L.N. Zakharov, M.R. Golder, R. Jasti, ACS Cent. Sci. 7 (2021) 1056-1065.
- [45] S. Wang, X. Li, X. Zhang, P. Huang, P. Fang, J. Wang, S. Yang, K. Wu, P. Du, Chem. Sci. 12 (2021) 10506–10513.
- [46] J. Wang, Y. Zhu, G. Zhuang, Y. Wu, S. Wang, P. Huang, G. Sheng, M. Chen, S. Yang, T. Greber, P. Du, Nat. Commun. 13 (2022) 1239.
- [47] D. Wu, W. Cheng, X. Ban, J. Xia, Asian J. Org. Chem. 7 (2018) 2161–2181.
 [48] G.-H. Zhong, X.-J. Chen, H.-Q. Lin, Front. Phys. 7 (2019) 52.
- [49] M.C. Stuparu, Acc. Chem. Res. 54 (2021), 2858-2370.
- [50] G.A. Leith, N.B. Shustova, Chem. Commun. 57 (2021) 10125-10138.
- [51] Z. Liu, S. Fu, X. Liu, A. Narita, P. Samorì, M. Bonn, H.I. Wang, Adv. Sci. 9 (2022) 2106055
- [52] D. Odkhuu, D. Jung, H. Lee, S.S. Han, S.-H. Choi, R. Ruoff, N. Park, Carbon 66 (2014) 39-47
- [53] R. Friedlein, X. Crispin, W.R. Salaneck, J. Power Sources 129 (2004) 29-33.
- [54] A. Omidvar, ACS Appl. Energy Mater. 3 (2020) 11463-11469.
- [55] R.E. Gerald, C.S. Johnson, J.W. Rathke, R.J. Klingler, G. Sandr, L.G. Scanlon, J. Power Sources 89 (2000) 237-243.
- [56] S. Sato, A. Unemoto, T. Ikeda, S.-I. Orimo, H. Isobe, Small 12 (2016) 3381-3387
- [57] H.J. Yen, H. Tsai, M. Zhou, E.F. Holby, S. Choudhury, A. Chen, L. Adamska, S. Tretiak, T. Sanchez, S. Iyer, H. Zhang, L. Zhu, H. Lin, L. Dai, G. Wu, H.L. Wang, Adv. Mater. 28 (2016) 10250-10256.
- [58] J. Park, C.W. Lee, S.H. Joo, J.H. Park, C. Hwang, H.-K. Song, Y.S. Park, S.K. Kwak, S. Ahn, S.J. Kang, J. Mater. Chem. A 6 (2018) 12589-12597.
- [59] A. Rajkamal, R. Thapa, Adv. Mater. Technol. 4 (2019) 1900307.
- [60] J. Qu, X.-X. Dai, J.-S. Cui, R.-X. Chen, X. Wang, Y.-H. Lin, R. Verduzco, H.-L. Wang, J. Mater. Chem. A 9 (2021) 16554-16564.
- [61] T. Hayakawa, Y. Ishii, S. Kawasaki, RSC Adv. 6 (2016) 22069-22073.

- [62] D. He, F. Xiao, Z. Wang, A. He, R. Liu, G. Jin, Nanoscale Res. Lett. 14 (2019) 65.
- [63] A.C. Grimsdale, J. Wu, K. Müllen, Chem. Commun. (2005) 2197–2204.
- [64] R. Mitsuhashi, Y. Suzuki, Y. Yamanari, H. Mitamura, T. Kambe, N. Ikeda, H. Okamoto, A. Fujiwara, M. Yamaji, N. Kawasaki, Y. Maniwa, Y. Kubozono, Nature 464 (2010) 76-79.
- [65] X.F. Wang, R.H. Liu, Z. Gui, Y.L. Xie, Y.J. Yan, J.J. Ying, X.G. Luo, X.H. Chen, Nat. Commun. 2 (2011) 507.
- M. Xue, T. Cao, D. Wang, Y. Wu, H. Yang, X. Dong, J. He, F. Li, G.F. Chen, Sci. Rep. 2 (2012) 389.
- [67] G.A. Artioli, F. Hammerath, M.C. Mozzati, P. Carretta, F. Corana, B. Mannucci, S. Margadonna, L. Malavasi, Chem. Commun. 51 (2015) 1092-1095.
- [68] Y. Takabayashi, M. Menelaou, H. Tamura, N. Takemori, T. Koretsune, A. Štefančič, G. Klupp, A.J.C. Buurma, Y. Nomura, R. Arita, D. Arčon, M.J. Rosseinsky, K. Prassides, Nat. Chem. 9 (2017) 635-643.
- [69] T.A. Scott, B.A. Ooro, D.J. Collins, M. Shatruk, A. Yakovenko, K.R. Dunbar, H.-C. Zhou, Chem. Commun. (2009) 65-67.
- [70] M. Castillo, A.J. Metta-Magaña, S. Fortier, New J. Chem. 40 (2016) 1923-1926.
- [71] H. Bock, C. Arad, C. Näther, Z. Havlas, J. Chem. Soc., Chem. Commun. (1995) 2393-2394.
- H. Bock, K. Gharagozloo-Hubmann, M. Sievert, T. Prisner, Z. Havlas, Nature 404 (2000) 267-269.
- [73] S.V. Rosokha, J.K. Kochi, J. Org. Chem. 71 (2006) 9357-9365.
- [74] W. Jost, M. Adam, V. Enkelmann, K. Müllen, Angew. Chem. Int. Ed. 31 (1992)
- C. Näther, H. Bock, R.F.C. Claridge, Helv. Chim. Acta 79 (1996) 84-91.
- C. Näther, H. Bock, Z. Havlas, T. Hauck, Organometallics 17 (1998) 4707-4715.
- [77] H. Bock, R.F. Claridge, C. Bogdan, M. Sievert, V. Krenzel, Helv. Chim. Acta 84 2001) 1227-1242.
- H. Bock, C. Näther, Z. Havlas, J. Am. Chem. Soc. 117 (1995) 3869-3870.
- [79] H. Bock, K. Gharagozloo-Hubmann, S. Holl, M. Sievert, Z. Naturforsch, B: Chem. Sci. 55 (2000) 1163.
- [80] H. Bock, M. Sievert, C.L. Bogdan, B.O. Kolbesen, A. Wittershagen, Organometallics 18 (1999) 2387-2389.
- [81] J. Zhang, G.F.S. Whitehead, T.D. Manning, D. Stewart, C.I. Hiley, M.J. Pitcher, S. Jansat, K. Prassides, M.J. Rosseinsky, J. Am. Chem. Soc. 140 (2018) 18162-
- [82] H. Bock, C. Arad, C. Näther, J. Organomet. Chem. 520 (1996) 1-13.
- [83] D. Bladauski, W. Broser, H.-J. Hecht, D. Rewicki, H. Dietrich, Chem. Ber. 112 (1979) 1380-1391.
- [84] T. Wombacher, R. Goddard, C.W. Lehmann, J.J. Schneider, Chem. Commun. 53 (2017) 7030-7033.
- [85] T. Wombacher, R. Goddard, C.W. Lehmann, J.J. Schneider, Dalton Trans. 46 (2017) 14122-14129.
- [86] T. Wombacher, R. Goddard, C.W. Lehmann, I.I. Schneider, Dalton Trans. 47 (2018) 10874-10883.
- [87] M. Håkansson, C.-H. Ottosson, A. Boman, D. Johnels, Organometallics 17 (1998) 1208-1214.
- [88] D.E. Paul, D. Lipkin, S.I. Weissman, J. Am. Chem. Soc. 78 (1956) 116-120.
- [89] H. van Willigen, J.A.M. van Broekhoven, E. de Boer, Mol. Phys. 12 (1967) 533-
- [90] M.R.D. Stephen, B. Wagner, J.H. Freed, J. Chem. Phys. 52 (1970) 5404–5417.
- [91] M.R. Arick, J.A.M. Van Broekhoven, F.W. Pijpers, E. De Boer, J. Am. Chem. Soc. 94 (1972) 7531–7536.
- [92] R.E. Koning, H. Zandvoort, P.J. Zandstra, Chem. Phys. 28 (1978) 343-355.
- [93] K. Meerholz, J. Heinze, J. Am. Chem. Soc. 111 (1989) 2325-2326.
- [94] A. Devos, M. Lannoo, Phys. Rev. B 58 (1998) 8236–8239.
- [95] O. Lemaire, M. De Backer, A. Devos, F.X. Sauvage, Synth. Met. 123 (2001) 61-

- [96] M. Hatanaka, J. Mol. Struct.: THEOCHEM 915 (2009) 69–72.
 [97] R. Rieger, K. Müllen, J. Phys. Org. Chem. 23 (2010) 315–325.
 [98] X.-M. Zhao, G.-H. Zhong, J. Zhang, Q.-W. Huang, A.F. Goncharov, H.-Q. Lin, X.-J.
- Chen, Sci. Rep. 6 (2016) 25600.

 [99] A. Štefančić, G. Klupp, T. Knaflič, D.S. Yufit, G. Tavčar, A. Potočnik, A. Beeby, D. Arčon, J. Phys. Chem. C 121 (2017) 14864–14871.

 [100] Z. Zhou, Ö. Üngör, Z. Wei, M. Shatruk, A. Tsybizova, R. Gershoni-Poranne, M.A.
- Petrukhina, Inorg. Chem. 60 (2021) 14844-14853.

- [101] J.M. Robertson, J.G. White, Nature 154 (1944) 605.
 [102] J.M. Robertson, J.G. White, J. Chem. Soc. (1945) 607–617.
 [103] T.M. Krygowski, M. Cyrański, A. Ciesielski, B. Świrska, P. Leszczyński, J. Chem. Inf. Comput. Sci. 36 (1996) 1135–1141.
- [104] L.G. Scanlon, G. Sandi, J. Power Sources 81-82 (1999) 176-181.
- [105] H. Ruuska, T.A. Pakkanen, J. Phys. Chem. B 105 (2001) 9541–9547.
- [106] Y. Kubozono, H. Mitamura, X. Lee, X. He, Y. Yamanari, Y. Takahashi, Y. Suzuki, Y. Kaji, R. Eguchi, K. Akaike, T. Kambe, H. Okamoto, A. Fujiwara, T. Kato, T. Kosugi, H. Aoki, PhysChemChemPhys 13 (2011) 16476–16493.
- [107] T. Okazaki, Y. Iizumi, S. Okubo, H. Kataura, Z. Liu, K. Suenaga, Y. Tahara, M. Yudasaka, S. Okada, S. Iijima, Angew. Chem. Int. Ed. 50 (2011) 4853–4857.
- [108] L. Gross, F. Mohn, N. Moll, B. Schuler, A. Criado, E. Guitian, D. Pena, A. Gourdon, G. Meyer, Science 337 (2012) 1326–1329.
- [109] B.S. Jensen, V.D. Parker, J. Am. Chem. Soc. 97 (1975) 5211–5217.[110] S.N. Spisak, N.J. Sumner, A.V. Zabula, A.S. Filatov, A.Yu. Rogachev, M.A. Petrukhina, Organometallics 32 (2013) 3773-3779.
- [111] C. Janiak, H. Hemling, Chem. Ber. 127 (1994) 1251-1253.
- [112] A.V. Zabula, M.A. Petrukhina, Adv. Organomet. Chem. 61 (2013) 375-462.
- [113] L. Gherghel, J.D. Brand, M. Baumgarten, K. Müllen, J. Am. Chem. Soc. 121 (1999) 8104-8105.

- [114] P.T. Herwig, V. Enkelmann, O. Schmelz, K. Müllen, Chem. Eur. J. 6 (2000) 1834-1839
- [115] Z. Zhou, Z. Wei, X. Yao, X.-Y. Wang, K. Müllen, M. Jo, M. Shatruk, M.A. Petrukhina, Cryst. Growth Des. 23 (2023) 1189-1194.
- T. Sugawara, M.M. Matsushita, J. Mater. Chem. 19 (2009) 1738-1753.
- [117] I. Choudhuri, P. Bhauriyal, B. Pathak, Chem. Mater. 31 (2019) 8260-8285.
- [118] R. Rabelo, S.-E. Stiriba, D. Cangussu, C. Pereira, N. Moliner, R. Ruiz-García, J. Cano, J. Faus, Y. Journaux, M. Julve, Magnetochemistry 6 (2020) 69.
- [119] C. Yuste, M. Castellano, J. Ferrando-Soria, S.-E. Stiriba, N. Marino, M. Julve, F. Lloret, R. Ruiz-García, J. Cano, J. Coord. Chem. 75 (2022) 2359-2383.
- [120] M.A. Petrukhina, L.T. Scott, Dalton Trans. (2005) 2969–2975.
- [121] M.A. Petrukhina, Coord. Chem. Rev. 251 (2007) 1690-1698.
- [122] A.S. Filatov, M.A. Petrukhina, Coord. Chem. Rev. 254 (2010) 2234–2246.
- [123] X.-Q. Hou, Y.-T. Sun, L. Liu, S.-T. Wang, R.-L. Geng, X.-F. Shao, Chin. Chem. Lett. 27 (2016) 1166-1174.
- [124] K. Kanagaraj, K. Lin, W. Wu, G. Gao, Z. Zhong, D. Su, C. Yang, Symmetry 9 (2017) 174.
- [125] M.A. Majewski, M. Stepien, Angew. Chem. Int. Ed. 58 (2019) 86-116.
- [126] A. Ayalon, M. Rabinovitz, P.-C. Cheng, L.T. Scott, Angew. Chem. Int. Ed. 31 (1992) 1636-1637.
- [127] A. Ayalon, A. Sygula, P.-C. Cheng, M. Rabinovitz, P.W. Rabideau, L.T. Scott, Science 265 (1994) 1065-1067
- [128] M. Baumgarten, L. Gherghel, M. Wagner, A. Weitz, M. Rabinovitz, P.C. Cheng, L.T. Scott, J. Am. Chem. Soc. 117 (1995) 6254–6257.
- [129] A.V. Zabula, S.N. Spisak, A.S. Filatov, A.Yu. Rogachev, M.A. Petrukhina, Acc. Chem. Res. 51 (2018) 1541-1549.
- [130] R.D. Shannon, Acta Crystallogr., Sect. A 32 (1976) 751-767.
- S.N. Spisak, A.V. Zabula, A.S. Filatov, A.Yu. Rogachev, M.A. Petrukhina, Angew. Chem. Int. Ed. 50 (2011) 8090-8094.
- [132] S.N. Spisak, A.V. Zabula, A.S. Filatov, M.A. Petrukhina, J. Organomet. Chem. 784 (2015) 69–74.
- [133] A.Yu. Rogachev, S. Liu, Q. Xu, J. Li, Z. Zhou, S.N. Spisak, Z. Wei, M.A. Petrukhina, Organometallics 38 (2019) 552-566.
- [134] A.V. Zabula, S.N. Spisak, A.S. Filatov, A.Yu. Rogachev, R. Clérac, M.A. Petrukhina, Chem. Sci. 7 (2016) 1954-1961.
- [135] S.N. Spisak, A.Yu. Rogachev, A.V. Zabula, A.S. Filatov, R. Clérac, M.A. Petrukhina, Chem. Sci. 8 (2017) 3137–3145.
- [136] A.V. Zabula, A.S. Filatov, S.N. Spisak, A.Yu. Rogachev, M.A. Petrukhina, Science 333 (2011) 1008-1011.
- [137] A.V. Zabula, S.N. Spisak, A.S. Filatov, M.A. Petrukhina, Organometallics 31 (2012) 5541-5545.
- [138] A.S. Filatov, A.V. Zabula, S.N. Spisak, A.Yu. Rogachev, M.A. Petrukhina, Angew. Chem. Int. Ed. 53 (2014) 140–145.
- [139] A.S. Filatov, S.N. Spisak, A.V. Zabula, J. McNeely, A.Yu. Rogachev, M.A. Petrukhina, Chem. Sci. 6 (2015) 1959–1966.
- [140] S.N. Spisak, Z. Wei, M.A. Petrukhina, Dalton Trans. 46 (2017) 5625-5630.
- [141] I. Aprahamian, R.E. Hoffman, T. Sheradsky, D.V. Preda, M. Bancu, L.T. Scott, M.
- Rabinovitz, Angew. Chem. Int. Ed. 41 (2002) 1712–1715. [142] I. Aprahamian, D.V. Preda, M. Bancu, A.P. Belanger, T. Sheradsky, L.T. Scott, M. Rabinovitz, J. Org. Chem. 71 (2006) 290-298.
- [143] N. Treitel, T. Sheradsky, L. Peng, L.T. Scott, M. Rabinovitz, Angew. Chem. Int. Ed. 45 (2006) 3273-3277.
- [144] S.N. Spisak, Z. Wei, N.J. O'Neil, A.Yu. Rogachev, T. Amaya, T. Hirao, M.A. Petrukhina, J. Am. Chem. Soc. 137 (2015) 9768-9771. [145] S.N. Spisak, Z. Wei, A.Yu. Rogachev, T. Amaya, T. Hirao, M.A. Petrukhina,
- Angew. Chem. Int. Ed. 56 (2017) 2582-2587. [146] S.N. Spisak, J. Li, A.Yu. Rogachev, Z. Wei, T. Amaya, T. Hirao, M.A. Petrukhina,
- Organometallics 36 (2017) 4961-4967.
- [147] Z. Zhou, Z. Wei, T. Hirao, T. Amaya, M.A. Petrukhina, Organometallics 40 (2021) 2023–2026.
- [148] K.Y. Amsharov, M.A. Kabdulov, M. Jansen, Angew. Chem. Int. Ed. 51 (2012) 4594-4597
- [149] S.N. Spisak, J. Li, A.Yu. Rogachev, Z. Wei, O. Papaianina, K. Amsharov, A.V. Rybalchenko, A.A. Goryunkov, M.A. Petrukhina, Organometallics 35 (2016) 3105-3111.
- [150] Z. Zhou, S.N. Spisak, Q. Xu, A.Yu. Rogachev, Z. Wei, M. Marcaccio, M.A. Petrukhina, Chem. Eur. J. 24 (2018) 3455.
 [151] Z. Zhou, Z. Wei, Y. Tokimaru, S. Ito, K. Nozaki, M.A. Petrukhina, Angew. Chem.
- Int. Ed. 58 (2019) 12107-12111
- [152] B. Li, C. Yang, X. Wang, G. Li, W. Peng, H. Xiao, S. Luo, S. Xie, J. Wu, Z. Zeng, Angew. Chem. Int. Ed. 60 (2021) 19790-19796.
- [153] A.V. Zabula, S.N. Spisak, A.S. Filatov, V.M. Grigoryants, M.A. Petrukhina, Chem. Eur. J. 18 (2012) 6476-6484. [154] S.N. Spisak, A.V. Zabula, M.V. Ferguson, A.S. Filatov, M.A. Petrukhina,
- Organometallics 32 (2013) 538-543. [155] A.V. Zabula, S.N. Spisak, A.S. Filatov, M.A. Petrukhina, Angew. Chem. Int. Ed.
- 51 (2012) 12194-12198. [156] M.A. Petrukhina, Dalton Trans. 48 (2019) 5125-5130.
- [157] J. Cai, P. Ruffieux, R. Jaafar, M. Bieri, T. Braun, S. Blankenburg, M. Muoth, A.P. Seitsonen, M. Saleh, X. Feng, K. Müllen, R. Fasel, Nature 466 (2010) 470-473.
- [158] A. Narita, X.-Y. Wang, X. Feng, K. Müllen, Chem. Soc. Rev. 44 (2015) 6616-6643.
- [159] M. Ball, Y. Zhong, Y. Wu, C. Schenck, F. Ng, M. Steigerwald, S. Xiao, C. Nuckolls, Acc. Chem. Res. 48 (2015) 267-276.
- [160] H. Ito, K. Ozaki, K. Itami, Angew. Chem. Int. Ed. 56 (2017) 11144–11164.
- [161] I.V. Alabugin, E. Gonzalez-Rodriguez, Acc. Chem. Res. 51 (2018) 1206-1219.

- [162] C. Zeng, B. Wang, H. Zhang, M. Sun, L. Huang, Y. Gu, Z. Qiu, K. Müllen, C. Gu, Y. Ma, J. Am. Chem. Soc. 143 (2021) 2682-2687.
- [163] W. Matsuoka, H. Ito, D. Sarlah, K. Itami, Nat. Commun. 12 (2021) 3940.
- [164] Y. Gu, Z. Qiu, K. Müllen, J. Am. Chem. Soc. 144 (2022) 11499–11524.
- [165] A. Borissov, Y.K. Maurya, L. Moshniaha, W.-S. Wong, M. Żyła-Karwowska, M. Stępień, Chem. Rev. 122 (2022) 565-788.
- [166] T. Kirschbaum, F. Rominger, M. Mastalerz, Angew. Chem. Int. Ed. 59 (2020) 270-274.
- [167] M.A. Medel, C.M. Cruz, D. Miguel, V. Blanco, S.P. Morcillo, A.G. Campaña, Angew. Chem. Int. Ed. 60 (2021) 22051-22056.
- [168] P. Liu, X.-Y. Chen, J. Cao, L. Ruppenthal, J.M. Gottfried, K. Müllen, X.-Y. Wang, J. Am. Chem. Soc. 143 (2021) 5314-5318.
- [169] K. Kato, K. Takaba, S. Maki-Yonekura, N. Mitoma, Y. Nakanishi, T. Nishihara, T. Hatakeyama, T. Kawada, Y. Hijikata, J. Pirillo, L.T. Scott, K. Yonekura, Y. Segawa, K. Itami, J. Am. Chem. Soc. 143 (2021) 5465–5469.
- [170] Y. Fei, Y. Fu, X. Bai, L. Du, Z. Li, H. Komber, K.H. Low, S. Zhou, D.L. Phillips, X. Feng, J. Liu, J. Am. Chem. Soc. 143 (2021) 2353–2360.
- [171] B. Ejlli, P. Nußbaum, F. Rominger, J. Freudenberg, U.H.F. Bunz, K. Müllen, Angew. Chem. Int. Ed. 60 (2021) 20220–20224.
- [172] R. Kumar, P. Chmielewski, T. Lis, D. Volkmer, M. Stępień, Angew. Chem. Int. Ed. 61 (2022) e202207486.
- [173] M. Krzeszewski, Ł. Dobrzycki, A.L. Sobolewski, M.K. Cyrański, D.T. Gryko, Chem. Sci. 14 (2023) 2353-2360.
- [174] W. Wang, X.-H. Ma, M. Liu, S. Tang, X. Ding, Y. Zhao, Y. Tan, M. Kertesz, X. Wang, Angew. Chem. Int. Ed. 62 (2023) e202217788.

- [175] J.M. Fernandez-Garcia, P.J. Evans, S. Medina Rivero, I. Fernandez, D. Garcia-Fresnadillo, J. Perles, J. Casado, N. Martín, J. Am. Chem. Soc. 140 (2018) 17188-17196.
- [176] Z. Zhou, Y. Zhu, J.M. Fernández-García, Z. Wei, I. Fernández, M.A. Petrukhina,
- N. Martín, Chem. Commun. 58 (2022) 5574–5577. [177] S.N. Spisak, Z. Zhou, S. Liu, Q. Xu, Z. Wei, K. Kato, Y. Segawa, K. Itami, A.Yu. Rogachev, M.A. Petrukhina, Angew. Chem. Int. Ed. 60 (2021) 25445–25453.
- [178] M. Müller, V.S. Iyer, C. Kübel, V. Enkelmann, K. Müllen, Angew. Chem. Int. Ed. 36 (1997) 1607–1610.
- [179] Z. Zhou, Y. Zhu, Z. Wei, J. Bergner, C. Neiß, S. Doloczki, A. Görling, M. Kivala, M. A. Petrukhina, Angew. Chem. Int. Ed. 60 (2021) 3510-3514.
- [180] S.H. Pun, Y. Wang, M. Chu, C.K. Chan, Y. Li, Z. Liu, Q. Miao, J. Am. Chem. Soc. 141 (2019) 9680-9686.
- [181] Y. Zhang, Y. Zhu, D. Lan, S.H. Pun, Z. Zhou, Z. Wei, Y. Wang, H.K. Lee, C. Lin, J. Wang, M.A. Petrukhina, Q. Li, Q. Miao, J. Am. Chem. Soc. 143 (2021) 5231-5238
- [182] Z. Zhou, X.-Y. Wang, Z. Wei, K. Müllen, M.A. Petrukhina, Angew. Chem. Int. Ed. 58 (2019) 14969-14973.
- [183] Z. Zhou, L. Fu, Y. Hu, X.Y. Wang, Z. Wei, A. Narita, K. Müllen, M.A. Petrukhina, Angew. Chem. Int. Ed. 59 (2020) 15923-15927.
- [184] Z. Zhou, J.M. Fernández-García, Y. Zhu, P.J. Evans, R. Rodríguez, J. Crassous, Z. Wei, I. Fernández, M.A. Petrukhina, N. Martín, Angew. Chem. Int. Ed. 61 (2022) e202115747.